Development (2014) 141, 2260-2270 doi:10.1242/dev.103705

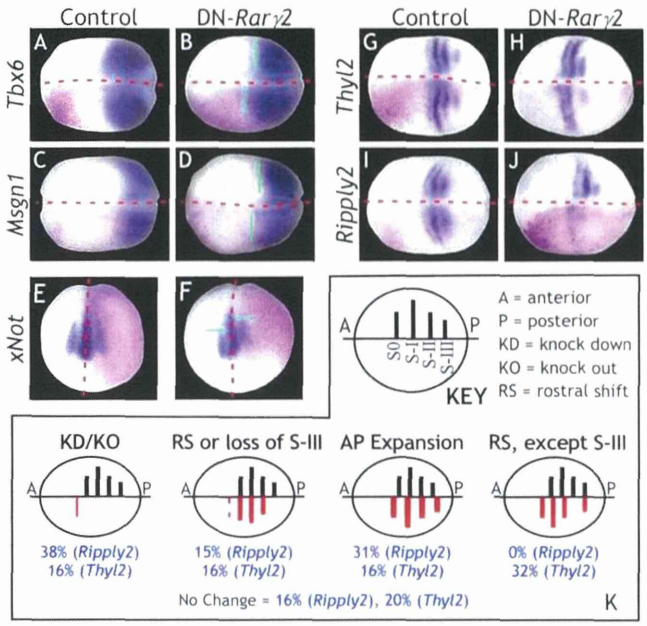

Fig. 8. Overexpression of DN-*Rarγ2* mRNA expands expression of PSM and CNH markers, shifting or knocking down somitomere markers *Thyl2* and *Ripply2*. (A-J) Embryos injected unilaterally at 2- or 4-cell stage. Injected side is indicated by magenta β-gal lineage tracer. (A,C,E,G,I) Control (*mCherry*) mRNA does not alter expression of *Tbx6*, *Msgn1*, *Thyl2*, *Ripply2* or *xNot*. (B,D,F) 2 ng DN-*Rarγ2* mRNA expands expression of *Msgn1* (8/11) and *Tbx6* (15/23) (green lines) and rostrally shifts *xNot* (8/10). (H,J) DN-*Rarγ2* overexpression produces multiple phenotypes of *Thyl2* and *Ripply2* expression, as characterized and scored in K. Neurula embryos shown in dorsal view with anterior to left.

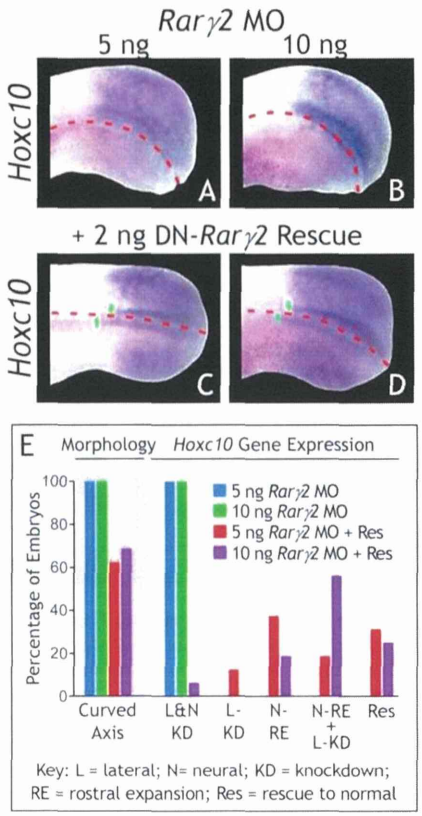

Fig. 9. DN-*Rarγ2* mRNA rescues posterior Hox expression in *Rarγ2* MO embryos. (A-D) Embryos injected unilaterally at 2- or 4-cell stage. Injected side is indicated by magenta β-gal lineage tracer. (A) 2.5 ng *Rarγ2.1* MO +2.5 ng *Rarγ2.2* MO or (B) 5 ng *Rarγ2.1* MO+5 ng *Rarγ2.2* MO diminishes *Hoxc10* expression and curves the embryo axis. (C,D) 2 ng DN-*Rarγ2* mRNA partially rescues this effect and expands neural expression of *Hoxc10*. Tailbud embryos shown in dorsal view with anterior to left. (E) Detailed scoring of the rescue experiment.

repression. However, we note distinct differences in the effects of 4647 on *Tbx6* versus *Msgn1*. *Tbx6* is upregulated by 4647 at early stages but downregulated at later stages, as also observed for the T-box gene *Tbx1* (Janesick et al., 2012). Unlike *Msgn1*, *Tbx6* plays a dual role in the unsegmented PSM and the determination front where it controls the anteroposterior patterning of somitomeres via *Ripply2* (Hitachi et al., 2008).

Msgn1 expression does not overlap somitomeres and functions to maintain unsegmented PSM by encouraging the differentiation of caudal stem cells. Loss of *Msgn1* expression leads to smaller somitomeres owing to the accumulation of bipotential progenitor cells that have not received signals to commit to PSM fate (Fior et al., 2012; Yabe and Takada, 2012). Treatment with 4647 also leads to loss of *Msgn1* and thus somitomeres should be smaller; however, they are larger. Despite such divergent early stage phenotypes, *Msgn1*$^{-/-}$ embryos (Yoon and Wold, 2000) and 4647 embryos both display fewer somites and reduced caudal structures at late stages. Caudal progenitors cannot be instructed to become somites in *Msgn1*$^{-/-}$ embryos. In 4647-treated embryos, the pool is expeditiously transformed into thickened somitomeres early, but the progenitor supply is exhausted before axial elongation is complete, reducing somitomere numbers. That 4647 can differentiate somitomeres at all without *Msgn1* is intriguing. Either *Tbx6* compensates for *Msgn1* knockdown, or 4647 can induce uncommitted, non-PSM progenitor cells to differentiate into somitomeres.

Relief of RARγ repression suppresses PSM and CNH marker gene expression

If RARγ2 functions solely as a repressor, then RARγ2 knockdown should induce a loss of repression phenotype. *Rarγ2* MO microinjection resulted in severely truncated body axes with caudal PSM and posterior Hox markers significantly reduced at tailbud stages, similar to 4647 treatment. This phenotype was attributed to axial defects, not merely developmental delay. We noted three differences between 4647-treated and *Rarγ2* MO-injected embryos. First, axes of *Rarγ2* MO embryos were significantly curved, which was attributed to imbalance/dominance of the uninjected side versus the truncated injected side. Second, caudal PSM markers, while qualitatively reduced with *Rarγ2* MO, also expanded rostrally, even when accounting for shortened axes on injected sides. Third, thickened, posteriorly expanded somitomeres were not seen with *Rarγ2* MO. RARγ2 acting as an activator near the somitogenesis front where RA is present would explain some discrepancies. RA functions in the determination wavefront to antagonize proliferating PSM and promote somitomere differentiation (Moreno and Kintner, 2004). If RA acts through RARγ2 in the wavefront, then loss of *Rarγ2* should expand unsegmented PSM and reduce somitomere expression, exactly as observed.

Axial curvature and loss of *Hoxc10* and *Msgn1* expression in *Rarγ2* MO-injected embryos could be rescued by *Rarγ2*, but not *Rarα2* or *Rarβ2* mRNA. Therefore, *Rarγ2* is the sole receptor responsible for axial elongation, in agreement with *Rarγ2* as the only RAR expressed in caudal domains. *Rarβ2* is present only in trunk and pharyngeal arches (Escriva et al., 2006) and *Rarα2* is completely absent from the blastopore and surrounding area (see figure S1A,B in the supplementary material of Janesick et al.,

Development (2014) 141, 2260-2270 doi:10.1242/dev.103705

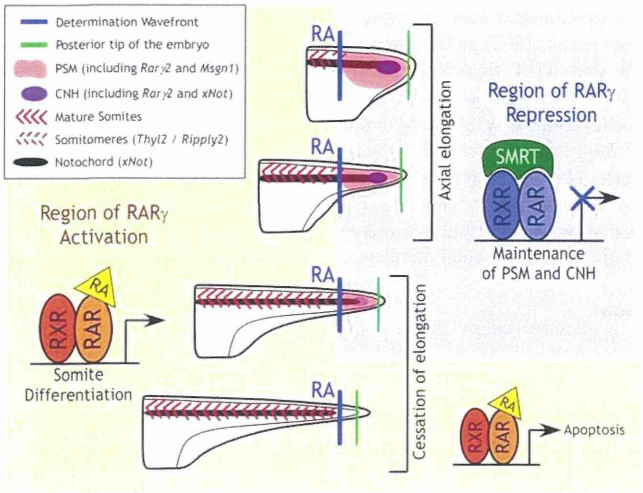

Fig. 10. RARγ functions as both transcriptional activator and repressor during somitogenesis and axial elongation. RARγ is activated by RA near the determination wavefront where PSM differentiates into somitomeres, then mature somites. The progenitor pool within the PSM and CNH domains, which is maintained by *Rarγ* repression, feeds into the wavefront until exhausted, as somitogenesis proceeds faster than progenitors are replenished (Gomez and Pourquie, 2009). As PSM and CNH domains diminish, the distance between RA/wavefront (blue line) and the posterior tip of the embryo (green line) becomes shorter. RA is able to enter the posterior, activating *Rarγ*, switching its function from repressor promoting growth to activator terminating growth. RXR, retinoid X receptor.

2013). *Hoxc10* expression could be rescued in *Rarγ2* MO-injected embryos by co-injecting DN-*Rarγ2* mRNA, definitively establishing that RARγ2 functions as a repressor in the caudal domain. DN-RARγ2 restored *Hoxc10* expression, especially in neural tube, where additional rostral expansion was often observed. DN-RARγ2 rescue restored curved axes only partially. We predict that axial curvature is a loss-of-activation effect inhibiting somitomere formation; therefore, the phenotype should not be rescued by DN-RARγ2, but rescued by wild-type RARγ2, as we observed.

Perhaps the most direct method for relieving repression of RARγ2 in caudal regions is overexpression of dominant-negative co-repressor c-SMRT, which binds RARγ2 preventing recruitment of co-repressors and thereby blocking repression. c-SMRT overexpression resulted in truncated axes with loss of posterior Hox, unsegmented PSM and CNH markers, but not rostral shifting of *Msgn1* and *Tbx6* as had been observed for *Rarγ2* MO embryos. This indicates that rostral shifting in *Rarγ2* MO embryos results from loss of activation rather than relief of repression. We previously showed that c-SMRT not only relieves repression of RAR but also potentiates ligand-mediated activation (Koide et al., 2001). Since c-SMRT was expressed ubiquitously, it could superactivate RARα or RARγ where RA is present. It should also be noted that c-SMRT can interact with other nuclear receptors and transcription factors. Therefore, we can only conclude that c-SMRT overexpression inhibits maintenance of the caudal PSM and progenitor pool (where RA is absent). We cannot draw conclusions about somitomere markers in c-SMRT overexpression embryos since their expression is controlled by RAR activation, which c-SMRT does not reduce.

RAR signaling and posterior Hox gene regulation

We identified a novel function for RARγ as a transcriptional repressor in the regulation of posterior Hox genes. Posterior Hox genes pattern caudal embryonic regions, promote axial elongation (Young et al., 2009) and are linked to cell cycle progression (Gabellini et al., 2003) and therefore proliferation. Axial elongation involves the addition of tissue, as cells must proliferate to contribute segments. Normally, FGF and RA signaling are mutually antagonistic, but we provide evidence that RARγ can support proliferative mechanisms in the absence of RA.

Hox gene expression was altered by 4647 and 5099 treatment, even post-gastrulation. Hence, although Hox gene expression is initiated collinearly during gastrulation, this temporal pattern is not immutable. In support of this model, axial progenitor cells transplanted to anterior locations do not retain their previous Hox identity (McGrew et al., 2008). Furthermore, manipulation of anteroposterior locations of PSM and the determination wavefront resulted in corresponding changes in Hox gene expression (Iimura et al., 2009; Wellik, 2007). We showed that 4647 treatment pushes determination fronts caudally and observed posterior regressions of *Hoxc10*, *Hoxd10* and *Hoxc13* expression. Conversely, rostral expansion in PSM by increasing RAR repression was accompanied by anterior shifts in posterior Hox expression. Owing to posterior prevalence, rostral shifts of *Hoxc10* or *Hoxd10* expression could indicate that thoracic segments will develop caudal structures at later stages. Similarly, rostral shifts in *Hoxc13* could drive lumbar segments to sacral morphology. Homeotic transformations from manipulating RAR repression deserve future study.

Conclusions

We conclude that the RAR-mediated repression of caudal genes is crucial for axial elongation, establishing another important role for active repression by nuclear receptors in body axis extension, as previously shown for head formation (Koide et al., 2001). RARγ2 is likely to function as an activator near the determination wavefront and a repressor to maintain axial progenitor pools in the PSM and CNH. As axial elongation nears completion, RARγ2 functions as an activator because the progenitor pool is exhausted and RA comes into close proximity to the caudal domain of RARγ2, where it can then promote apoptosis and terminate the body axis. This model is attractive because it utilizes the same protein to activate or repress target genes depending on the proximity to RA and explains the high levels of posterior RARγ2 expression. RARγ2 is likely to function in multiple steps of somitogenesis and axial elongation (Fig. 10): (1) preservation of undifferentiated states in the progenitor pools (marked by the CNH); (2) maintenance of PSM; (3) initiation of somitomere differentiation; and (4) axial termination. Future studies require RARγ target gene identification because very few ChIP studies have ascertained direct targets, and even fewer studies have explored subtype-selective RAR targets. In the case of inverse agonist-upregulated genes (the focal point of our study), identifying repressors of PSM and progenitors will be key, as these genes are likely to be targeted by unliganded RAR in a classic 'repression of a repressor' mechanism.

MATERIALS AND METHODS

Percellome microarray analysis

Xenopus laevis eggs from three different females were fertilized *in vitro* and embryos staged as described (Janesick et al., 2012). Stage 7 embryos were treated in groups of 25 in 60-mm Petri dishes with 10 ml 0.1× MBS containing 1 μM RAR agonist (TTNPB), 1 μM RAR inverse agonist (AGN193109) or vehicle control (0.1% ethanol). Three dishes per treatment per female were collected (27 dishes total: three technical replicates, three biological replicates per treatment). Each dish of embryos was harvested at stage 18 into 1.5 ml RNAlater (Invitrogen) and stored at 4°C. Samples were homogenized, RNA isolated and DNA quantitated (Kanno et al., 2006). Graded-dose spiked cocktail

Development (2014) 141, 2260-2270 doi:10.1242/dev.103705

(GSC) made of five *Bacillus subtilis* RNA sequences present on Affymetrix GeneChip arrays (AFFX-ThrX-3_at, AFFX-LysX-3_at, AFFX-PheX-3_at, AFFX-DapX-3_at, AFFX-TrpnX-3_at) was added to the sample homogenates in proportion to their DNA concentration (Kanno et al., 2006). GSC-spiked sample homogenates were processed and probes synthesized using standard Affymetrix protocols, applied to *Xenopus* microarray v1.0 GeneChips and analyzed using Percellome software (Kanno et al., 2006). Absolutized mRNA levels were expressed as copy number per cell for each probe set.

Percellome microarray data were analyzed using CyberT (Kayala and Baldi, 2012). We did not use low value thresholding/offsetting or log/VSN normalizations. Bayesian analysis used a sliding window of 101 and confidence value of 10. The *P*-values reported are Bonferroni corrected and Benjamini and Hochber corrected. The full microarray dataset is available at GEO under accession number GSE57352. Genes included in Table 1 comprise a subset upregulated by AGN193109/downregulated by TTNPB based on their regional expression in the posterior.

Embryo microinjection

Xenopus eggs were fertilized *in vitro* and embryos staged as described (Janesick et al., 2012). Embryos were injected bilaterally or unilaterally at the 2- or 4-cell stage with gene-specific morpholinos (MOs) (supplementary material Table S1) and/or mRNA together with 100 pg/embryo β-galactosidase (β-gal) mRNA. For all MO experiments, control embryos were injected with 10 ng standard control MO (GeneTools). Embryos were maintained in 0.1× MBS until appropriate stages. Embryos processed for WISH were fixed in MEMFA, stained with magenta-GAL (Biosynth), and then stored in 100% ethanol (Janesick et al., 2012).

pCDG1-DN-*xRarγ2* was constructed by cloning amino acids 1-393 (lacking the AF-2 domain) into the *Nco*I-*Bam*HI site of pCDG1 (Blumberg et al., 1998). pCDG1-VP16-*xRarγ2* was constructed by cloning the VP16 activation domain upstream of *xRarγ2* into pCDG1. pCDG1-*xRarα2*, pCMX-GAL4-*Rarα* and GAL4-*Rarγ* were from Blumberg et al. (Blumberg et al., 1996). *X. laevis Rarβ1* and *Rarβ2* sequences were found by aligning to the *X. tropicalis* sequences. pCDG1-*xRarβ2* and pCMX-GAL4-*xRarβ* cloning primers are listed in supplementary material Table S2. pCDG1-*xCyp26a1* and pCDG1-*c-smrt* were constructed by PCR amplification of *xCyp26a1* coding regions (Hollemann et al., 1998) or Xl *c-smrt* (37b−, 41+) (Chen et al., 1996; Malartre et al., 2004) and cloning into pCDG1.

xRarα1$^{EGCKG\rightarrow GSCKV}$, *xRarα2*$^{EGCKG\rightarrow GSCKV}$, *xRarβ2*$^{EGCKG\rightarrow GSCKV}$, *xRarγ1*$^{EGCKG\rightarrow GSCKV}$ and *xRarγ2*$^{EGCKG\rightarrow GSCKV}$ were designed according to Klein et al. (1996), constructed by two-fragment PCR, and cloned into pCDG1 (primer sequences are provided in supplementary material Table S3). Four copies of RXRE$^{1/2}$-GRE$^{1/2}$ (GGAAGGGTTCACCGAA-AGAACACTCGC) were cloned upstream of the TK-luciferase reporter. All pCDG1 plasmids were sequence verified, linearized with *Not*I, and mRNA transcribed using mMessage mMachine T7 (Ambion). pCS2-*mCherry* was linearized with *Not*I and transcribed from the SP6 promoter.

Embryo treatments and reporter assays

Microinjected embryos were treated at stage 8 with the following chemicals (in 0.1× MBS): TTNPB (RAR agonist), NRX204647 (RARγ-selective agonist), NRX205099 (RARγ-selective inverse agonist) or 0.1% ethanol vehicle. Twenty-five embryos were treated in each 60-mm Petri dish containing 10 ml chemical. Treated embryos were fixed in MEMFA and processed for WISH, or separated into five-embryo aliquots at stage 10.5 for luciferase assays, or separated into five-embryo aliquots at neurula or tailbud stage for QPCR as described (Janesick et al., 2012). Each group of five embryos was considered one biological replicate (n=1).

WISH

Embryos were microinjected or treated with chemicals after the completion of gastrulation (stage 12.5). WISH was performed as previously described (Janesick et al., 2012). *Rarγ1*, *Rarγ2*, *Rarα* (Blumberg et al., 1992), *Hoxc10*, *Ripply2*, *Thyl2*, *Msgn1* (Klein et al., 2002), *Hoxd10* (Lombardo and Slack, 2001), *Tbx6* (Uchiyama et al., 2001), *Raldh2* (Glinka et al., 1996) and *Myod* (Hopwood et al., 1989) probes were prepared by PCR amplification of coding regions from cDNA with T7 promoter at the 3′ end and *in vitro* transcribed. *Hoxc13* sequence was derived from EST clone XL042b19. Relevant primers are listed in supplementary material Table S4. *Krox20* (Bradley et al., 1993) and *En2* (Bolce et al., 1992) probes were made using T7 and T3 polymerase from *Eco*RI and *Xba*I linearized plasmids, respectively. Probes were transcribed with MEGAscript T7 (Ambion) in the presence of digoxigenin-11-UTP (Roche). Double WISH was conducted as described (Janesick et al., 2012). DNP-*Rarγ2* was transcribed in the presence of dinitrophenol-11-UTP (PerkinElmer). *Hoxc10* expression was quantitated using MATLAB (MathWorks) (supplementary material Fig. S8). The number of purple pixels was calculated by thresholding individual RGB channels (R&B>170, G>120) and dividing by the total number of pixels occupied by the embryo.

Transfection

1 µg CMX-*Rar*$^{EGCKG\rightarrow GSCKV}$ effector plasmid was co-transfected with 5 µg tk-(RXRE$^{1/2}$-GRE$^{1/2}$)×4 luciferase reporter and 5 µg pCMX-β-galactosidase transfection control plasmids as previously described (Chamorro-Garcia et al., 2012). For activation assays, NRX204647 was tested from 10^{-11} M to 10^{-5} M. For antagonism assays, NRX205099 was tested from 10^{-10} M to 10^{-5} M against 10^{-8} M 9-cis RA. All transfections were performed in triplicate and reproduced in multiple experiments. Data are reported as normalized luciferase±s.e.m. or percentage reduction±s.e.m. using standard propagation of error (Bevington and Robinson, 2003).

Quantitative real-time reverse transcription PCR (QPCR)

Total RNA from five-embryo pools was DNase treated, LiCl precipitated, and reverse transcribed into cDNA (Janesick et al., 2012). First-strand cDNA was quantitated in a Light Cycler 480 System (Roche) using primer sets listed in supplementary material Table S5 and SYBR Green. Each primer set amplified a single band as determined by gel electrophoresis and melting curve analysis. QPCR data for supplementary material Figs S2 and S7 were analyzed by ΔCt relative to *Histone H4*, correcting for amplification efficiency between RARs (Pfaffl, 2001). QPCR data for supplementary material Figs S11 and S12 were analyzed by ΔΔCt relative to *Histone H4*, normalizing to control embryos. Error bars represent biological replicates calculated using standard propagation of error.

Acknowledgements

We thank Connie Chung for technical help during the early stages of this study and Dr Dennis Bittner for editorial assistance.

Competing interests

The authors declare no competing financial interests.

Author contributions

T.T.L.N. performed WISH. K.A., K.I., S.K. and J.K. executed the Percellome microarray experiment. R.A.S.C. provided 4647 and 5099 chemicals with advice on use. A.J. and B.B. designed, supervised and performed experiments, and wrote, edited and submitted the manuscript.

Funding

Supported by grants from the National Science Foundation (NSF) [IOS-0719576, IOS-1147236 to B.B.]. A.J. was a predoctoral trainee of NSF IGERT DGE 0549479. K.I., S.K. and J.K. were funded by Health Sciences Research Grant H15-kagaku-002 from the Ministry of Health, Labour and Welfare, Japan.

Supplementary material

Supplementary material available online at
http://dev.biologists.org/lookup/suppl/doi:10.1242/dev.103705/-/DC1

References

Abu-Abed, S., Dollé, P., Metzger, D., Beckett, B., Chambon, P. and Petkovich, M. (2001). The retinoic acid-metabolizing enzyme, CYP26A1, is essential for normal hindbrain patterning, vertebral identity, and development of posterior structures. *Genes Dev.* **15**, 226-240.

Arima, K., Shiotsugu, J., Niu, R., Khandpur, R., Martinez, M., Shin, Y., Koide, T., Cho, K. W. Y., Kitayama, A., Ueno, N. et al. (2005). Global analysis of RAR-responsive genes in the Xenopus neurula using cDNA microarrays. *Dev. Dyn.* **232**, 414-431.

Beck, C. W. and Slack, J. M. W. (1998). Analysis of the developing Xenopus tail bud reveals separate phases of gene expression during determination and outgrowth. *Mech. Dev.* **72**, 41-52.

Bevington, P. R. and Robinson, D. K. (2003). *Data Reduction and Error Analysis for the Physical Sciences*. New York: McGraw-Hill Education.

Development (2014) 141, 2260-2270 doi:10.1242/dev.103705

Blewitt, R. (2009). Enhancer of split-related-2 mRNA shows cyclic expression during somitogenesis in Xenopus laevis. *Biosci. Horizons* **2**, 22-31.

Blumberg, B., Mangelsdorf, D. J., Dyck, J. A., Bittner, D. A., Evans, R. M. and De Robertis, E. M. (1992). Multiple retinoid-responsive receptors in a single cell: families of retinoid "X" receptors and retinoic acid receptors in the Xenopus egg. *Proc. Natl. Acad. Sci. U.S.A.* **89**, 2321-2325.

Blumberg, B., Bolado, J., Jr, Derguini, F., Craig, A. G., Moreno, T. A., Chakravarti, D., Heyman, R. A., Buck, J. and Evans, R. M. (1996). Novel retinoic acid receptor ligands in Xenopus embryos. *Proc. Natl. Acad. Sci. U.S.A.* **93**, 4873-4878.

Blumberg, B., Bolado, J., Jr, Moreno, T. A., Kintner, C., Evans, R. M. and Papalopulu, N. (1997). An essential role for retinoid signaling in anteroposterior neural patterning. *Development* **124**, 373-379.

Blumberg, B., Kang, H., Bolado, J., Chen, H., Craig, A. G., Moreno, T. A., Umesono, K., Perlmann, T., De Robertis, E. M. and Evans, R. M. (1998). BXR, an embryonic orphan nuclear receptor activated by a novel class of endogenous benzoate metabolites. *Genes Dev.* **12**, 1269-1277.

Bolce, M. E., Hemmati-Brivanlou, A., Kushner, P. D. and Harland, R. M. (1992). Ventral ectoderm of Xenopus forms neural tissue, including hindbrain, in response to activin. *Development* **115**, 681-688.

Bradley, L. C., Snape, A., Bhatt, S. and Wilkinson, D. G. (1993). The structure and expression of the Xenopus Krox-20 gene: conserved and divergent patterns of expression in rhombomeres and neural crest. *Mech. Dev.* **40**, 73-84.

Buchberger, A., Bonneick, S. and Arnold, H.-H. (2000). Expression of the novel basic-helix-loop-helix transcription factor cMespo in presomitic mesoderm of chicken embryos. *Mech. Dev.* **97**, 223-226.

Cambray, N. and Wilson, V. (2002). Axial progenitors with extensive potency are localised to the mouse chordoneural hinge. *Development* **129**, 4855-4866.

Cambray, N. and Wilson, V. (2007). Two distinct sources for a population of maturing axial progenitors. *Development* **134**, 2829-2840.

Chakravarti, D., LaMorte, V. J., Nelson, M. C., Nakajima, T., Schulman, I. G., Juguilon, H., Montminy, M. and Evans, R. M. (1996). Role of CBP/P300 in nuclear receptor signalling. *Nature* **383**, 99-103.

Chamorro-García, R., Kirchner, S., Li, X., Janesick, A., Casey, S. C., Chow, C. and Blumberg, B. (2012). Bisphenol A diglycidyl ether induces adipogenic differentiation of multipotent stromal stem cells through a peroxisome proliferator-activated receptor gamma-independent mechanism. *Environ. Health Perspect.* **120**, 984-989.

Chen, J. D. and Evans, R. M. (1995). A transcriptional co-repressor that interacts with nuclear hormone receptors. *Nature* **377**, 454-457.

Chen, J. D., Umesono, K. and Evans, R. M. (1996). SMRT isoforms mediate repression and anti-repression of nuclear receptor heterodimers. *Proc. Natl. Acad. Sci. U.S.A.* **93**, 7567-7571.

Dahmann, C., Oates, A. C. and Brand, M. (2011). Boundary formation and maintenance in tissue development. *Nat. Rev. Genet.* **12**, 43-55.

Davis, R. L. and Kirschner, M. W. (2000). The fate of cells in the tailbud of Xenopus laevis. *Development* **127**, 255-267.

de Roos, K., Sonneveld, E., Compaan, B., ten Berge, D., Durston, A. J. and van der Saag, P. T. (1999). Expression of retinoic acid 4-hydroxylase (CYP26) during mouse and Xenopus laevis embryogenesis. *Mech. Dev.* **82**, 205-211.

Dequéant, M.-L. and Pourquié, O. (2008). Segmental patterning of the vertebrate embryonic axis. *Nat. Rev. Genet.* **9**, 370-382.

Dubrulle, J., McGrew, M. J. and Pourquié, O. (2001). FGF signaling controls somite boundary position and regulates segmentation clock control of spatiotemporal Hox gene activation. *Cell* **106**, 219-232.

Escriva, H., Bertrand, S., Germain, P., Robinson-Rechavi, M., Umbhauer, M., Cartry, J., Duffraisse, M., Holland, L., Gronemeyer, H. and Laudet, V. (2006). Neofunctionalization in vertebrates: the example of retinoic acid receptors. *PLoS Genet.* **2**, e102.

Fior, R., Maxwell, A. A., Ma, T. P., Vezzaro, A., Moens, C. B., Amacher, S. L., Lewis, J. and Saude, L. (2012). The differentiation and movement of presomitic mesoderm progenitor cells are controlled by Mesogenin 1. *Development* **139**, 4656-4665.

Fujii, H., Sato, T., Kaneko, S., Gotoh, O., Fujii-Kuriyama, Y., Osawa, K., Kato, S. and Hamada, H. (1997). Metabolic inactivation of retinoic acid by a novel P450 differentially expressed in developing mouse embryos. *EMBO J.* **16**, 4163-4173.

Gabellini, D., Colaluca, I. N., Vodermaier, H. C., Biamonti, G., Giacca, M., Falaschi, A., Riva, S. and Peverali, F. A. (2003). Early mitotic degradation of the homeoprotein HOXC10 is potentially linked to cell cycle progression. *EMBO J.* **22**, 3715-3724.

Glinka, A., Delius, H., Blumenstock, C. and Niehrs, C. (1996). Combinatorial signalling by Xwnt-11 and Xnr3 in the organizer epithelium. *Mech. Dev.* **60**, 221-231.

Gomez, C. and Pourquié, O. (2009). Developmental control of segment numbers in vertebrates. *J. Exp. Zool. B Mol. Dev. Evol.* **312B**, 533-544.

Hitachi, K., Kondow, A., Danno, H., Inui, M., Uchiyama, H. and Asashima, M. (2008). Tbx6, Thylacine1, and E47 synergistically activate bowline expression in Xenopus somitogenesis. *Dev. Biol.* **313**, 816-828.

Hollemann, T., Chen, Y., Grunz, H. and Pieler, T. (1998). Regionalized metabolic activity establishes boundaries of retinoic acid signalling. *EMBO J.* **17**, 7361-7372.

Hopwood, N. D., Pluck, A. and Gurdon, J. B. (1989). MyoD expression in the forming somites is an early response to mesoderm induction in Xenopus embryos. *EMBO J.* **8**, 3409-3417.

Iimura, T., Denans, N. and Pourquié, O. (2009). Establishment of Hox vertebral identities in the embryonic spine precursors. *Curr. Top. Dev. Biol.* **88**, 201-234.

Janesick, A., Shiotsugu, J., Taketani, M. and Blumberg, B. (2012). RIPPLY3 is a retinoic acid-inducible repressor required for setting the borders of the pre-placodal ectoderm. *Development* **139**, 1213-1224.

Janesick, A., Abbey, R., Chung, C., Liu, S., Taketani, M. and Blumberg, B. (2013). ERF and ETV3L are retinoic acid-inducible repressors required for primary neurogenesis. *Development* **140**, 3095-3106.

Kanno, J., Aisaki, K.-i., Igarashi, K., Nakatsu, N., Ono, A., Kodama, Y. and Nagao, T. (2006). "Per cell" normalization method for mRNA measurement by quantitative PCR and microarrays. *BMC Genomics* **7**, 64.

Kayala, M. A. and Baldi, P. (2012). Cyber-T web server: differential analysis of high-throughput data. *Nucleic Acids Res.* **40**, W553-W559.

Klein, E. S., Pino, M. E., Johnson, A. T., Davies, P. J. A., Nagpal, S., Thacher, S. M., Krasinski, G. and Chandraratna, R. A. S. (1996). Identification and functional separation of retinoic acid receptor neutral antagonists and inverse agonists. *J. Biol. Chem.* **271**, 22692-22696.

Klein, S. L., Strausberg, R. L., Wagner, L., Pontius, J., Clifton, S. W. and Richardson, P. (2002). Genetic and genomic tools for Xenopus research: the NIH Xenopus initiative. *Dev. Dyn.* **225**, 384-391.

Koide, T., Downes, M., Chandraratna, R. A. S., Blumberg, B. and Umesono, K. (2001). Active repression of RAR signaling is required for head formation. *Genes Dev.* **15**, 2111-2121.

Lamka, M. L., Boulet, A. M. and Sakonju, S. (1992). Ectopic expression of UBX and ABD-B proteins during Drosophila embryogenesis: competition, not a functional hierarchy, explains phenotypic suppression. *Development* **116**, 841-854.

Leroy, P., Nakshatri, H. and Chambon, P. (1991). Mouse retinoic acid receptor alpha 2 isoform is transcribed from a promoter that contains a retinoic acid response element. *Proc. Natl. Acad. Sci. U.S.A.* **88**, 10138-10142.

Lombardo, A. and Slack, J. M. (2001). Abdominal B-type Hox gene expression in Xenopus laevis. *Mech. Dev.* **106**, 191-195.

Malartre, M., Short, S. and Sharpe, C. (2004). Alternative splicing generates multiple SMRT transcripts encoding conserved repressor domains linked to variable transcription factor interaction domains. *Nucleic Acids Res.* **32**, 4676-4686.

McGrew, M. J., Sherman, A., Lillico, S. G., Ellard, F. M., Radcliffe, P. A., Gilhooley, H. J., Mitrophanous, K. A., Cambray, N., Wilson, V. and Sang, H. (2008). Localised axial progenitor cell populations in the avian tail bud are not committed to a posterior Hox identity. *Development* **135**, 2289-2299.

Mollard, R., Viville, S., Ward, S. J., Décimo, D., Chambon, P. and Dollé, P. (2000). Tissue-specific expression of retinoic acid receptor isoform transcripts in the mouse embryo. *Mech. Dev.* **94**, 223-232.

Moreno, T. A. and Kintner, C. (2004). Regulation of segmental patterning by retinoic acid signaling during Xenopus somitogenesis. *Dev. Cell* **6**, 205-218.

Nakaya, Y., Kuroda, S., Katagiri, Y. T., Kaibuchi, K. and Takahashi, Y. (2004). Mesenchymal-epithelial transition during somitic segmentation is regulated by differential roles of Cdc42 and Rac1. *Dev. Cell* **7**, 425-438.

Nowotschin, S., Ferrer-Vaquer, A., Concepcion, D., Papaioannou, V. E. and Hadjantonakis, A.-K. (2012). Interaction of Wnt3a, Msgn1 and Tbx6 in neural versus paraxial mesoderm lineage commitment and paraxial mesoderm differentiation in the mouse embryo. *Dev. Biol.* **367**, 1-14.

Olivera-Martinez, I., Harada, H., Halley, P. A. and Storey, K. G. (2012). Loss of FGF-dependent mesoderm identity and rise of endogenous retinoid signalling determine cessation of body axis elongation. *PLoS Biol.* **10**, e1001415.

Pfaffl, M. W. (2001). A new mathematical model for relative quantification in real-time RT-PCR. *Nucleic Acids Res.* **29**, e45.

Pfeffer, P. L. and De Robertis, E. M. (1994). Regional specificity of RAR gamma isoforms in Xenopus development. *Mech. Dev.* **45**, 147-153.

Pourquié, O. and Tam, P. P. L. (2001). A nomenclature for prospective somites and phases of cyclic gene expression in the presomitic mesoderm. *Dev. Cell* **1**, 619-620.

Rhinn, M. and Dollé, P. (2012). Retinoic acid signalling during development. *Development* **139**, 843-858.

Sakai, Y., Meno, C., Fujii, H., Nishino, J., Shiratori, H., Saijoh, Y., Rossant, J. and Hamada, H. (2001). The retinoic acid-inactivating enzyme CYP26 is essential for establishing an uneven distribution of retinoic acid along the anterio-posterior axis within the mouse embryo. *Genes Dev.* **15**, 213-225.

Shimono, K., Tung, W.-e., Macolino, C., Chi, A. H.-T., Didizian, J. H., Mundy, C., Chandraratna, R. A., Mishina, Y., Enomoto-Iwamoto, M., Pacifici, M. et al. (2011). Potent inhibition of heterotopic ossification by nuclear retinoic acid receptor-gamma agonists. *Nat. Med.* **17**, 454-460.

Development (2014) 141, 2260-2270 doi:10.1242/dev.103705

Shum, A. S. W., Poon, L. L. M., Tang, W. W. T., Koide, T., Chan, B. W. H., Leung, Y.-C. G., Shiroishi, T. and Copp, A. J. (1999). Retinoic acid induces down-regulation of Wnt-3a, apoptosis and diversion of tail bud cells to a neural fate in the mouse embryo. *Mech. Dev.* **84**, 17-30.

Sive, H. L., Draper, B. W., Harland, R. M. and Weintraub, H. (1990). Identification of a retinoic acid-sensitive period during primary axis formation in Xenopus laevis. *Genes Dev.* **4**, 932-942.

Sucov, H. M., Murakami, K. K. and Evans, R. M. (1990). Characterization of an autoregulated response element in the mouse retinoic acid receptor type beta gene. *Proc. Natl. Acad. Sci. U.S.A.* **87**, 5392-5396.

Takemoto, T., Uchikawa, M., Yoshida, M., Bell, D. M., Lovell-Badge, R., Papaioannou, V. E. and Kondoh, H. (2011). Tbx6-dependent Sox2 regulation determines neural or mesodermal fate in axial stem cells. *Nature* **470**, 394-398.

Tam, P. P. L., Goldman, D., Camus, A. and Schoenwolf, G. C. (2000). 1 Early events of somitogenesis in higher vertebrates: allocation of precursor cells during gastrulation and the organization of a meristic pattern in the paraxial mesoderm. *Curr. Top. Dev. Biol.* **47**, 1-32.

Thacher, S. M., Vasudevan, J. and Chandraratna, R. A. S. (2000). Therapeutic applications for ligands of retinoid receptors. *Curr. Pharm. Des.* **6**, 25-58.

Tsang, K. Y., Sinha, S., Liu, X., Bhat, S. and Chandraratna, R., A. (2003). Disubstituted Chalcone Oximes Having Rar(Gamma)-Retinoid Receptor Antagonist Activity. European Patent Office.

Uchiyama, H., Kobayashi, T., Yamashita, A., Ohno, S. and Yabe, S. (2001). Cloning and characterization of the T-box gene Tbx6 in Xenopus laevis. *Dev. Growth Differ.* **43**, 657-669.

von Dassow, G., Schmidt, J. E. and Kimelman, D. (1993). Induction of the Xenopus organizer: expression and regulation of Xnot, a novel FGF and activin-regulated homeo box gene. *Genes Dev.* **7**, 355-366.

Wellik, D. M. (2007). Hox patterning of the vertebrate axial skeleton. *Dev. Dyn.* **236**, 2454-2463.

Weston, A. D., Blumberg, B. and Underhill, T. M. (2003). Active repression by unliganded retinoid receptors in development: less is sometimes more. *J. Cell Biol.* **161**, 223-228.

Wong, C. W. and Privalsky, M. L. (1998). Transcriptional silencing is defined by isoform- and heterodimer-specific interactions between nuclear hormone receptors and corepressors. *Mol. Cell. Biol.* **18**, 5724-5733.

Yabe, T. and Takada, S. (2012). Mesogenin causes embryonic mesoderm progenitors to differentiate during development of zebrafish tail somites. *Dev. Biol.* **370**, 213-222.

Yoon, J. K. and Wold, B. (2000). The bHLH regulator pMesogenin1 is required for maturation and segmentation of paraxial mesoderm. *Genes Dev.* **14**, 3204-3214.

Yoon, J. K., Moon, R. T. and Wold, B. (2000). The bHLH class protein pMesogenin1 can specify paraxial mesoderm phenotypes. *Dev. Biol.* **222**, 376-391.

Young, T., Rowland, J. E., van de Ven, C., Bialecka, M., Novoa, A., Carapuco, M., van Nes, J., de Graaff, W., Duluc, I., Freund, J.-N. et al. (2009). Cdx and Hox genes differentially regulate posterior axial growth in mammalian embryos. *Dev. Cell* **17**, 516-526.

RESEARCH ARTICLE

Molecular Reproduction & Development 82:218–231 (2015)

Expression of Focal Adhesion Kinase in Mouse Cumulus-Oocyte Complexes, and Effect of Phosphorylation at Tyr397 on Cumulus Expansion

JUN OHTAKE, MASAHIRO SAKURAI,* YUMI HOSHINO,* KENTARO TANEMURA, AND EIMEI SATO

Laboratory of Animal Reproduction, Graduate School of Agricultural Science, Tohoku University, Sendai, Japan

SUMMARY

We investigated the expression of focal adhesion kinase (FAK) in mouse cumulus–oocyte complexes (COCs), as well as the role of FAK phosphorylation at Tyr397 during oocyte maturation. The effect of inhibiting FAK phosphorylation at Tyr397 during in vitro maturation (IVM) on subsequent fertilization and preimplantation embryo development was also examined. Western blotting analyses revealed that total and Tyr397-phosphorylated FAK were expressed in vivo in both cumulus cells and oocytes. Immunocytochemical studies localized this kinase throughout the cytoplasm of cumulus cells and oocytes; in particular, Tyr397-phosphorylated FAK tended to accumulate in regions where cumulus cells contact each other. Interestingly, the in vivo level of Tyr397 phosphorylation in cumulus cells was significantly lower after compared to before cumulus expansion. Addition of FAK inhibitor 14, which specifically blocks phosphorylation at Tyr397, stimulated oocyte meiotic maturation and cumulus expansion during IVM in the absence of follicle-stimulating hormone (FSH). Reverse-transcriptase PCR showed that the mRNA expression of hyaluronan synthase 2 (*Has2*), a marker of cumulus expansion, was significantly induced in cumulus cells. Subsequent in vitro fertilization and culture showed that more oocytes developed to the blastocyst stage when they were treated with FAK inhibitor 14 during IVM, although the blastocyst total cell number was lower than in oocytes stimulated with FSH. These results indicate that FAK is involved in the maturation of COCs; specifically, phosphorylation at Tyr397 may regulate cumulus expansion via the expression of *Has2* mRNA in cumulus cells, which could affect the developmental competence of oocytes.

*Corresponding authors:
Laboratory of Animal Reproduction
Graduate School of Agricultural Science, Tohoku University, 1-1 Amamiyamachi, Tsutsumidori, Aoba-ku, Sendai 981-8555, Japan. E-mail: msaku913@gmail.com (M.S.), hoshimi@bios.tohoku.ac.jp (Y.H.)

Jun Ohtake and Masahiro Sakurai contributed equally to this work.

Grant sponsor: Japan Society for the Promotion of Science; Grant number: 24248047; Grant sponsor: Japan Society for the Promotion of Science JSPS KAKENHI; Grant number: 21780250, 26712022

Mol. Reprod. Dev. 82: 218–231, 2015. © *2015 Wiley Periodicals, Inc.*

Received 5 March 2014; Accepted 16 January 2015

Published online 18 February 2015 in Wiley Online Library (wileyonlinelibrary.com).
DOI 10.1002/mrd.22464

INTRODUCTION

The final events of oogenesis occur in large antral follicles, where the oocyte is intimately surrounded by supporting cumulus cells, forming cumulus -oocyte complexes (COCs). In this special niche-cumulus cells are tightly connected to each other and to the oocyte via cell adhesion complexes and gap junctions (Eppig, 1991; Kidder and Mhawi, 2002). The oocyte depends on these associated

Abbreviations: COCs, cumulus-oocyte complexes; EGF[R], epidermal growth factor [receptor]; ERK1/2, extracellular signaling-regulated kinase 1/2; FAK, focal adhesion kinase; FSH, follicle-stimulating hormone; GV, germinal vesicle; Has2, hyaluronan synthase 2; hCG, human chorionic gonadotropin; IVM, in vitro maturation; LH, luteinizing hormone; MI/II, metaphase I/II; PMSG, pregnant mare serum gonadotropin; SFK, SRC-family tyrosine kinase

cumulus cells for glucose metabolism and supplying pyruvate for energy production (Biggers et al., 1967; Gardner et al., 1996; Preis et al., 2005). Oocytes are arrested for an exceptionally long time in prophase I of meiosis, which is referred to as the germinal vesicle (GV) stage. Meiotic resumption is manifested by germinal vesicle breakdown (GVBD), which is followed by chromosome condensation and metaphasel (MI) spindle assembly; homologous chromosome segregation; and completion of the first meiotic division. Meiosis is arrested again at metaphase II (MII) until fertilization.

COCs expand dramatically during meiotic maturation in oocytes. This phenomenon, termed "cumulus expansion", occurs after the pre-ovulatory surge of gonadotropins, and is believed to support COC dissociation from the follicle wall and its expulsion through the ruptured follicle wall during ovulation (Chen et al., 1993). Cumulus expansion is essential for fertilization and the development of early embryos (Chen et al., 1993; Hess et al., 1999), and failure of these processes causes infertility (Russell and Robker 2007).

Compelling evidence from mouse studies has shown that the ovulatory surge of luteinizing hormone (LH) induces a rapid secondary cascade of epidermal growth factor (EGF)-like peptides (such as amphiregulin, epiregulin, β-cellulin, etc.) in the somatic cells of the follicle, leading to cumulus expansion, oocyte maturation, and ovulation (Park et al., 2004; Hsieh et al., 2007). These peptides act on granulosa and cumulus cells via EGF receptor (EGFR) (Park et al., 2004; Shimada et al., 2006; Noma et al., 2011). Binding of EGF stimulates EGFR tyrosine kinase activity, resulting in EGFR autophosphorylation and subsequent tyrosine phosphorylation of numerous substrates within the cell (Carpenter and Cohen, 1990). Insulin-like growth factor I, which binds to a tetrameric transmembrane receptor tyrosine kinase, efficiently reduces the apoptosis of cumulus cells cultured in vitro (Sirotkin et al., 2002) while stimulating the proliferation and terminal differentiation of cumulus cells during the expansion process (Khamsi and Armstrong, 1997). Nerve growth factor, whose tyrosine kinase receptor, TRKA, is also located in cumulus cells, induces marked cumulus expansion and progressive cumulus-oocyte uncoupling (Barboni et al., 2002).

In oocytes, on the other hand, SRC-family tyrosine kinases (SFKs), which are closely related both structurally and functionally (Thomas and Brugge, 1997), are expressed at much higher levels than in other cell types. *Fyn* and *Yes* transcripts, in particular, are more abundant in oocytes than in most other mammalian cell types (Luo et al., 2009). Antibodies specific for the catalytic domains of SFKs revealed that both inactive and active SFKs are closely associated with the meiotic spindle in mouse oocytes (McGinnis et al., 2007; Zheng et al., 2007). Therefore, tyrosine kinase activity is important for regulating oocyte meiotic maturation and cumulus expansion.

Focal adhesion kinase (FAK) is a non-receptor tyrosine kinase that plays a critical role in a variety of biological functions, including cell proliferation, spreading, motility, and survival or apoptosis (Schaller et al., 1992; Schwartz et al., 1995; Hanks and Polte, 1997; Chan et al., 1999; Sonoda et al., 2000; Wang et al., 2001; Goel and Dey, 2002). FAK is phosphorylated on tyrosine residues in response to integrin engagement, G protein-coupled receptor activation, and growth-factor receptor stimulation (Zachary and Rozengurt, 1992; Girault et al., 1999). Integrin-stimulated FAK phosphorylation, for example, is complex, and can occur at six or more sites in vivo: two sites within the FAK amino-terminal domain (Tyr397 and 407); two sites within the kinase domain activation loop (Tyr576 and 577); and two sites within carboxy-terminal domain (Tyr861 and 925) (Calalb et al., 1995; Schlaepfer and Hunter, 1996). Phosphorylation of Tyr397 generally occurs first, which allows binding of SH2 domains of SRC (Schaller et al., 1994), FYN (Cobb et al., 1994), or phosphatidylinositol 3-kinase (PI3K) (Chen et al., 1996). Recruitment of these SFKs stimulates phosphorylation of additional tyrosine residues (Schlaepfer et al., 1994; Calalb et al., 1995; Calalb et al., 1996). Phosphorylation at Tyr576 and 577 in the catalytic domain increases FAK activity (Calalb et al., 1995; Owen et al., 1999), while phosphorylation at Tyr925 can activate the RAS pathway and extracellular signaling-regulated kinase 1 and 2 (ERK1/2) (Schlaepfer et al., 1994). Binding of PI3K, on the other hand, activates the anti-apoptotic protein kinase B (PKB or AKT) pathway (Chen et al., 1996; Sonoda et al., 2000). In some cells, the SH2 domain of GRB2 binds to phosphorylated Tyr927 and triggers RAS-dependent activation of the mitogen-activated protein kinase (MAPK) pathway (Schlaepfer et al., 1994; Schlaepfer and Hunter, 1996). Adding to the complexity, FAK can be phosphorylated by SRC at Tyr407 and Tyr861 (Calalb et al., 1996). FAK could also play a scaffolding role mediating crosstalk between signaling pathways; for example, by inducing anchorage-dependent JNK activation in a kinase-independent fashion by interacting with paxillin (Igishi et al., 1999). Therefore, FAK phosphorylation on Tyr397 appears to be critical for both its activation and scaffolding function in vitro, the latter of which can trigger assembly of the multi-molecular complexes responsible for its cellular effects.

FAK is overexpressed in ovarian cancer, and its overabundance is predictive of poor clinical outcome (Judson et al., 1999; Sood et al., 2004). Yet, the role of FAK and its phosphorylation at Tyr397 in the normal ovary was not fully understood until recently. We demonstrated that total FAK and Tyr397-phosphorylated FAK are expressed in normal mouse ovaries, particularly enriched in granulosa cells of growing follicles where phosphorylation at Tyr397 is implicated in cellular survival (Sakurai et al., 2012). FAK protein abundance has been quantified in porcine oocytes (Pelech et al., 2008), and has been histologically proposed to function in pro-survival events (Okamura et al., 2001). Recently, FAK was shown to be expressed in mouse oocytes at the MII stage, and Tyr861-phosphorylated FAK was concentrated in the oocyte cortex following sperm incorporation and during anaphase, together implicating FAK in fertilization (McGinnis et al., 2013).

To our knowledge, the sequence of events from the LH surge to FAK phosphorylation has been revealed only in

mouse Leydig tumor cells: addition of human chorionic gonadotropin (hCG) to MA-10 cells expressing the endogenous LH receptor results in the phosphorylation of FAK at Tyr576 and Tyr577 and of paxillin, which is a downstream target of the FAK–SFK complexes (Mizutani et al., 2006). Detailed analyses of the expression and function of FAK, especially Tyr397-phosphorylated FAK, in COCs during oocyte maturation have not been conducted. Therefore, we examined the expression of FAK and the importance of phosphorylation at Tyr397 during oocyte maturation in mice. In addition, the developmental capability of oocytes treated with an FAK phosphorylation inhibitor during in vitro maturation (IVM) was evaluated by in vitro fertilization and subsequent in vitro culture of the resulting embryos.

RESULTS

In Vivo Expression and Distribution of Total FAK and Tyr397-Phosphorylated FAK in Cumulus Cells

We first examined the in vivo expression levels of total FAK and Tyr397-phosphorylated FAK in mouse cumulus cells before and after cumulus expansion at 0 or 12 hr after hCG treatment, respectively, following pregnant mare serum gonadotropin (PMSG) treatment. Western-blot analyses demonstrated that total FAK and Tyr397-phosphorylated FAK were present in cumulus cells (Fig. 1A; Supplemental Fig. S1). Interestingly, although the expression of total FAK before and after expansion did not differ, the abundance of Tyr397-phosphorylated FAK was significantly lower after cumulus expansion than before (Fig. 1B).

The distribution of total FAK and Tyr397-phosphorylated FAK in cumulus cells was analyzed by immunofluorescence staining of mouse COCs. During COC maturation, total FAK and Tyr397-phosphorylated FAK localized throughout the cell, with intense expression of Tyr397-phosphorylated FAK observed in regions of cell-cell contact (Fig. 1C). Lower FAK phosphorylation levels were similarly observed after cumulus expansion compared to before (Fig. 1C).

In Vivo Expression and Distribution of Total FAK and Tyr397-Phosphorylated FAK in Oocytes

The expression levels of total FAK and Tyr397-phosphorylated FAK were examined in vivo in GV- and MII-stage mouse oocytes, respectively 0 or 12 hr after hCG treatment. Western blot analyses demonstrated that total FAK and Tyr397-phosphorylated FAK were present in oocytes (Fig. 2A), and their expression levels did not differ between the two stages (Fig. 2B). Total and Tyr397-phosphorylated FAK resided in the cytoplasm, forming small punctate structures. This distribution pattern was the same when the oocytes were classified according to nuclear status (Fig. 2C), and total FAK distribution at MII is consistent with that in a previous report (McGinnis et al., 2013).

Inhibition of FAK Phosphorylation at Tyr397 During IVM: Effect on Oocyte Meiotic Maturation

To determine the function of FAK during oocyte meiotic maturation, we blocked FAK phosphorylation at Tyr397 during IVM using FAK inhibitor 14, which specifically and directly blocks phosphorylation at Tyr397 in a dose- and time-dependent manner. As FAK inhibitor 14 is known to induce non-apoptotic cell death by necrosis at 100 μM, thus decreasing the viability of cells (Golubovskaya et al., 2008), we first tested for any adverse effects it might have on oocytes by assessing the normality of nuclear status using α-tubulin immunostaining. Oocytes possessed degenerated nuclei after 18 hr of IVM in the presence of FSH and the inhibitor (Fig 3A). Compared to oocytes with normal nuclei and meiotic spindles (Fig 3A, upper panel), some oocytes treated with the inhibitor exhibited deformed GVs, abnormally shaped spindles, and nuclear condensation (Fig 3A, lower panel). Immunostaining for α-tubulin revealed that 92.6% of the untreated oocytes had typical MII spindles, and that treatment with 5 μM FAK inhibitor 14 during IVM did not adversely affect the oocytes, that is, 90.5% were at MII stage (Fig. 3B, white bar). In contrast, only 31.1 or 36.9% of oocytes treated with 10 or 25 μM inhibitor, respectively, had normal nuclei; but arrested between GV and MI stages (Fig. 3B, diagonal-line and dotted bars). Moreover, 17.6 or 63.3% of oocytes treated with 10 or 25 μM inhibitor, respectively, had degenerated nuclei (Fig. 3B, gray, cross-hatched, and black bars).

Detailed analysis of phenotypes at each dose of inhibitor revealed that increasing inhibitor concentration caused more adverse effects—that is, meiotic arrest with normal-shaped nuclei or nuclear degeneration—at earlier stages (Fig. 3B, non-white bars). Therefore, the number of oocytes that formed a normal-shaped MII spindle was significantly lower in oocytes treated with 10 and 25 μM inhibitor than in those treated with 0 and 5 μM inhibitor (Fig. 3B).

Effect of Inhibiting FAK Phosphorylation at Tyr397 During IVM on Cumulus Expansion

In general, the addition of FSH to IVM medium induces oocyte meiotic maturation and cumulus expansion. To analyze the effect of FAK phosphorylation at Tyr397 on cumulus expansion, we therefore added FAK inhibitor 14 to IVM medium that did not contain FSH. The diameter of the COCs was then measured by digital imaging at the end of the maturation period. Despite the absence of FSH, remarkable cumulus expansion was observed when FAK inhibitor 14 was added (Fig 4, upper panel); those cumulus cells that had fallen off during culture remained alive and adhered to the dish (Supplemental Fig. S2). Quantitative morphometric analyses (Fig. 4, graph) demonstrated that COC diameter was significantly larger in the presence of 5 or 10 μM FAK inhibitor 14 than in the absence of inhibitor, indicating that blocking FAK phosphorylation at Tyr397 can induce cumulus expansion. Indeed, 0.5 μM PF-562271, a different FAK inhibitor that blocks phosphorylation of

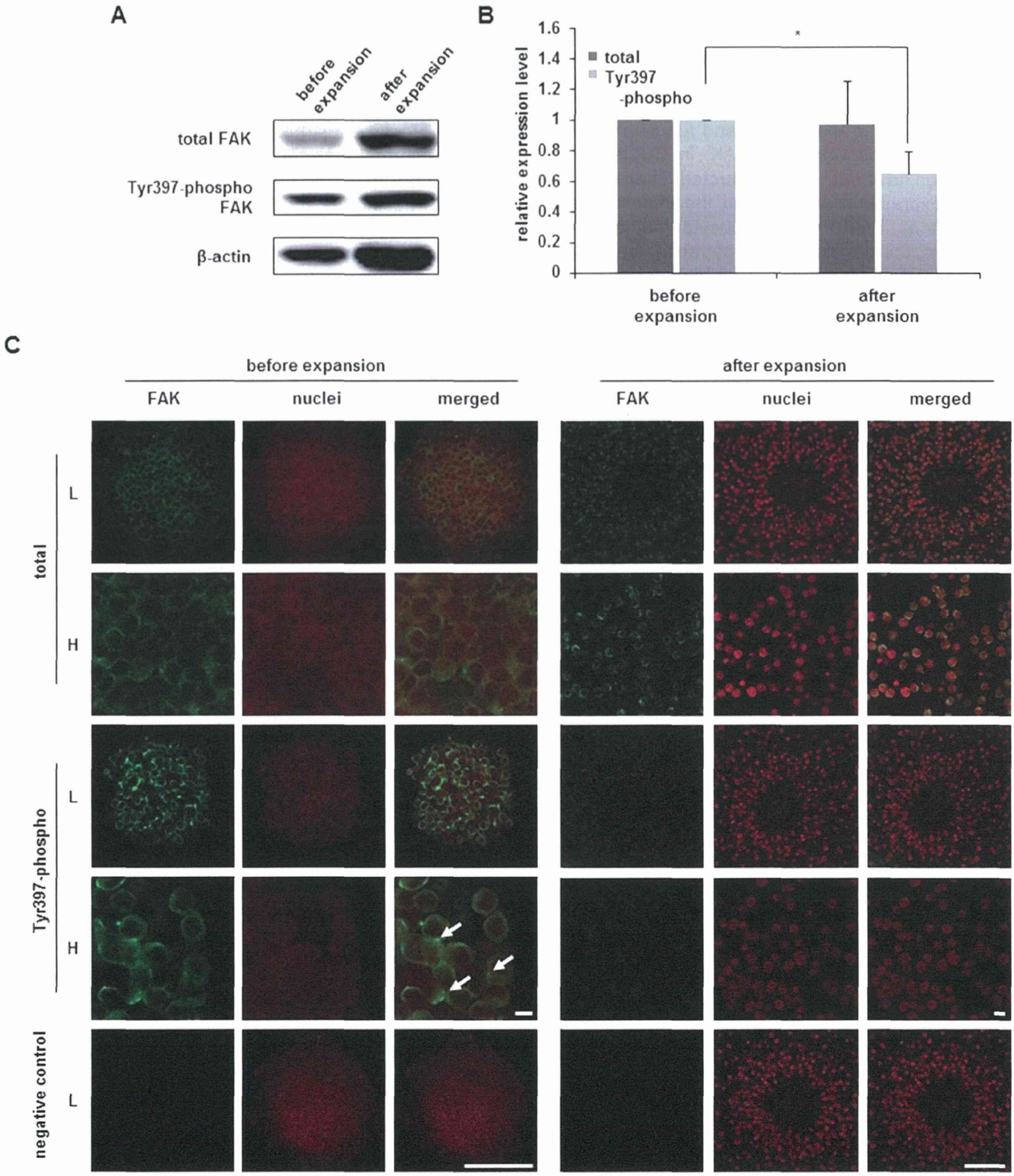

Figure 1. **A:** Expression of total FAK and Tyr397-phosphorylated FAK in cumulus cells before and after in vivo cumulus expansion. **B:** Relative expression of total and Tyr397-phosphorylated FAK protein. Values shown are the means ± standard deviations. A significant difference ($P < 0.01$) in Tyr397 phosphorylated FAK is indicated by an asterisk. **C:** Distribution of total and Tyr397-phosphorylated FAK in cumulus cells. COCs were immunostained for total and Tyr397-phosphorylated FAK with Alexa Fluor 488 (green) before (hCG 0 hr) and after (hCG 12 hr) cumulus expansion. Nuclei are shown in red. Arrows indicate the strong expression in the cell–cell contact regions. Scale bars, 50 μm/L. low-magnification; H, high-magnification.

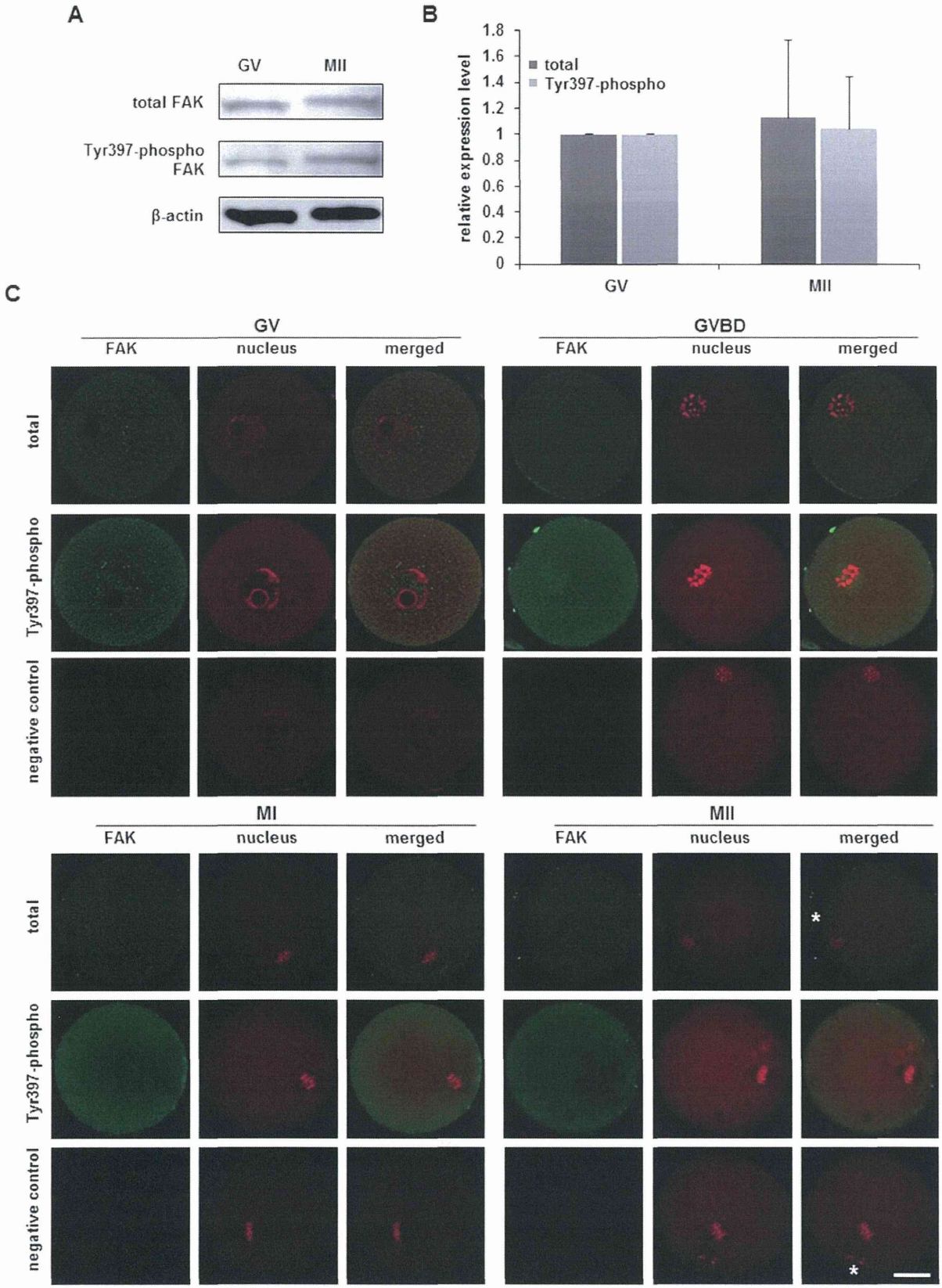

Figure 2. **A:** Expression of total FAK and Tyr397-phosphorylated FAK in in vivo-matured GV and MII oocytes. **B:** Relative expression of total and Tyr397-phosphorylated FAK. Values shown are the means ± standard deviations. **C:** Distribution of total and Tyr397-phosphorylated FAK in oocytes during meiotic maturation. Oocytes were immunostained for total and Tyr397-phosphorylated FAK with Alexa Fluor 488 (green). Nuclei are shown in red. Scale bars, 20 μm. COCs were collected at 0, 6, 10, and 18 hr after hCG for GV, GVBD, MI, and MII, respectively. Asterisks indicate the first polar body.

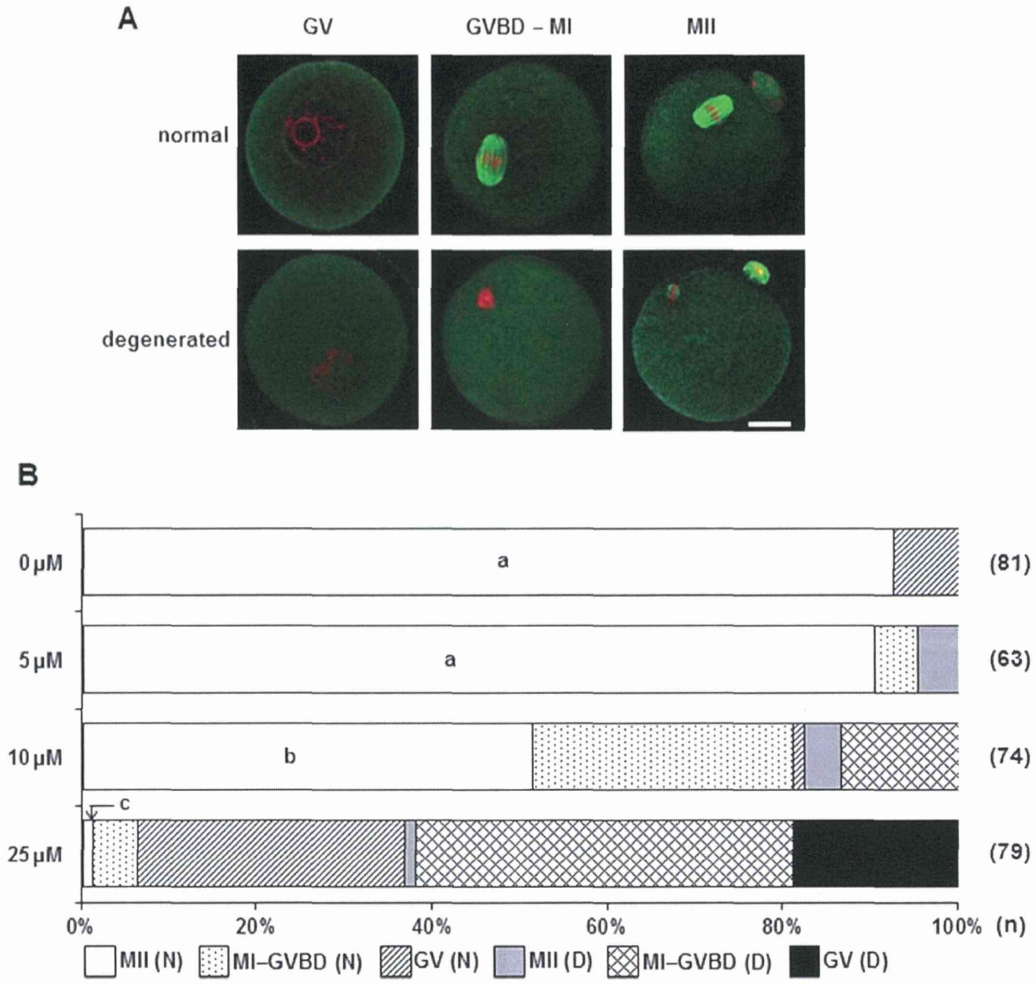

Figure 3. Effect of an FAK Tyr397 phosphorylation inhibitor on nuclear status. COCs at 48 hr after PMSG were matured in Waymouth's MB752/1 medium with FSH and increasing doses of FAK inhibitor 14 for 18 hr to specifically inhibit FAK phosphorylation at Tyr397, then immediately fixed for α-tubulin immunostaining. **A:** Normal or degenerated nucleus and the distribution of α-tubulin in mouse oocytes. Oocytes were immunostained for α-tubulin with Alexa Fluor 488 (green). Nuclei are shown in red. Scale bar, 20 μm. **B:** The percentage of oocytes at each meiotic stage with a normal (N) or degenerated (D) nucleus, according to FAK inhibitor concentration. Nuclei with normal morphology, but arrested between the GV and MI stage, were defined as abnormal (D). Values with different superscripts (a–c) are significantly different ($P < 0.05$) in the frequency of MII oocytes. Numbers in parentheses indicate the number of oocytes tested per group.

Tyr397, also induced cumulus expansion when added to the IVM medium, (Supplemental Fig. S3). Moreover, both inhibitors decreased levels of phospho-Tyr397 FAK prior to cumulus expansion (Supplemental Fig. S4).

Effect of Inhibiting FAK Phosphorylation at Tyr397 During IVM on *Has2* Transcription

Cumulus expansion is induced by the synthesis and secretion of hyaluronan-enriched extracellular matrix by cumulus cells, which is regulated by hyaluronan synthase 2 (HAS2) (Fulop et al., 1997). We therefore measured the abundance of *Has2* mRNA in cumulus cells to determine if the effect of FAK phosphorylation at Tyr397 on cumulus expansion was related to *Has2* expression. Semi-quantitative analysis indicated that *Has2* mRNA abundance was significantly higher in cumulus cells cultured in IVM medium containing 5 μM FAK inhibitor 14 than in cells cultured in IVM medium without inhibitor (Fig. 5; Supplemental Fig. S5), implying a positive effect of lower Tyr397 phosphorylation.

FAK Phosphorylation at Tyr397 Regulates the Maturation and Development of Oocytes

Finally, we investigated the maturation of oocytes in COCs expanded by FAK inhibitor 14, and their developmental competence, by performing in vitro fertilization followed by culturing. Based on the titration curve shown above, we determined that the optimum concentration of inhibitor 14 to be 5 μM; at this concentration, cumulus expansion was effectively induced with no adverse effects on oocyte meiotic maturation. As expected, the omission of FSH decreased the rate of oocytes reaching MII, although some oocytes spontaneously matured. In contrast, the addition of 0–5 μM FAK inhibitor 14 induced oocyte maturation without FSH in a

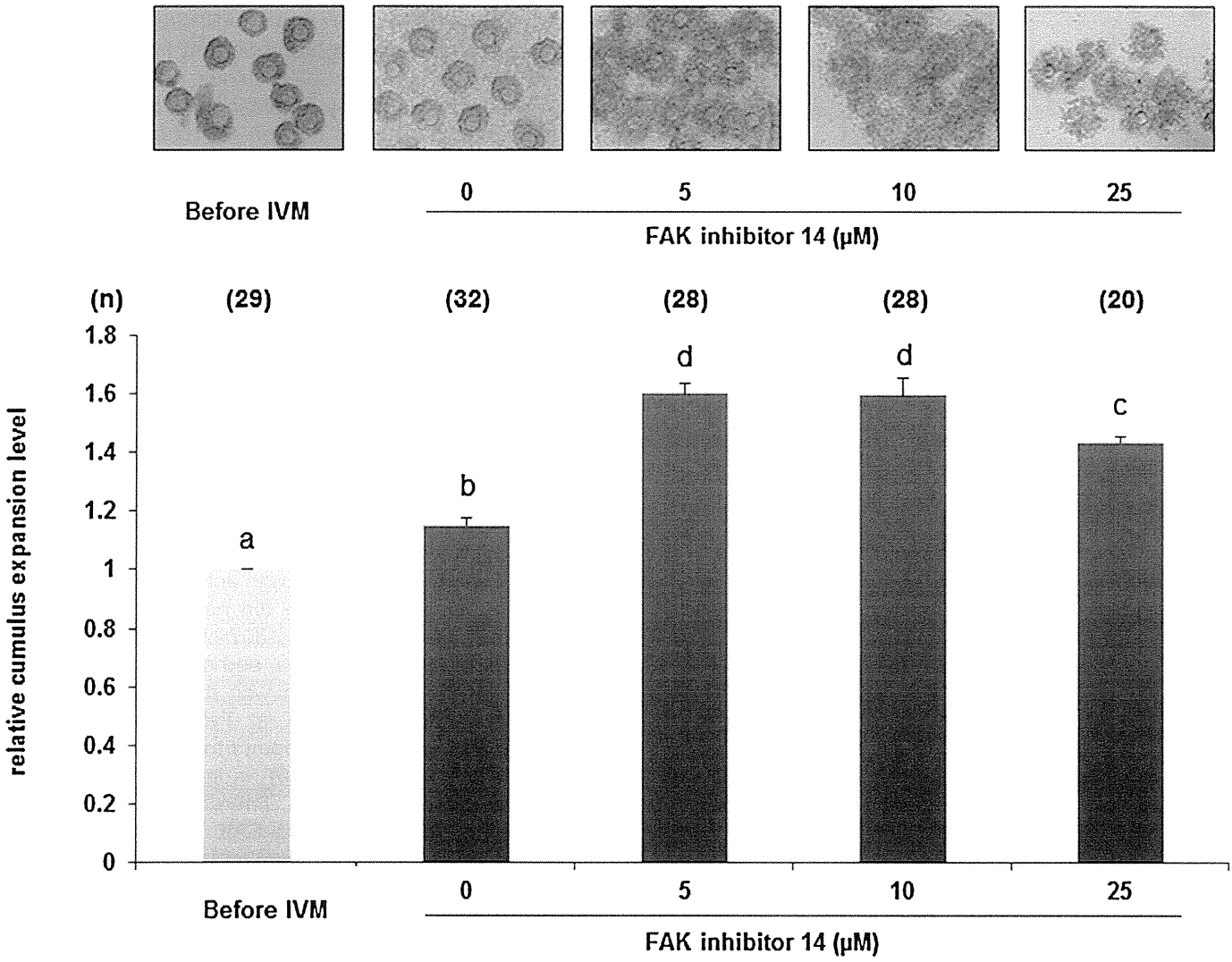

Figure 4. Effect of a FAK Tyr397 phosphorylation inhibitor on cumulus expansion. The upper panel shows COCs cultured with increasing doses of FAK inhibitor 14 without FSH for 18 hr. The lower bar graph shows the relative cumulus-expansion level of COCs. Values shown are the means ± standard deviations. Values with different superscripts (a–d) are significantly different ($P < 0.01$). Numbers in parentheses indicate the number of COCs tested per group.

dose-dependent manner, with the rate of MII oocytes significantly higher at 5 μM than in the absence of inhibitor (Fig. 6A). The addition of FAK inhibitor 14 to the IVM medium had no significant effect on fertilization rate after in vitro fertilization (Fig. 6B). In contrast, the rate of blastocyst formation of oocytes cultured with 5 μM FAK inhibitor 14 was significantly higher than that of oocytes cultured without inhibitor, but lower than those cultured with FSH (Fig. 6C). Total cell numbers in the blastocysts were lower in the blastocysts treated with FAK inhibitor 14 during IVM than in the blastocysts stimulated with FSH (Fig. 6D).

DISCUSSION

FAK is highly enriched in focal adhesions (Schaller et al., 1992; Hanks and Polte, 1997), and can regulate several cellular processes, such as cell proliferation and migration (Mitra et al., 2005), in response to extracellular stimuli (e.g., signals from the extracellularl matrix). FAK is required for the efficient assembly and disassembly of adhesions (Owen et al., 2007). Its dephosphorylation at Tyr397 is rapidly observed during integrin endocytosis and focal adhesion turnover, which occur during cellular detachment from an extracellular matrix (Nagano et al., 2012). In this study, strong expression of Tyr397-phosphorylated FAK was detected at cell-contact regions of cumulus cells, which suggest its possible function in the intercellular adhesion of the cumulus layer. This specific localization suggested that decreased phosphorylation of FAK at Tyr397, but not total FAK abundance, may participate in the disassembly of cumulus cells during cumulus expansion.

Localization and abundance of total FAK and Try397-phosphorylated FAK in the oocyte cytoplasm during meiotic maturation, specifically at the GV and MII stages, did not

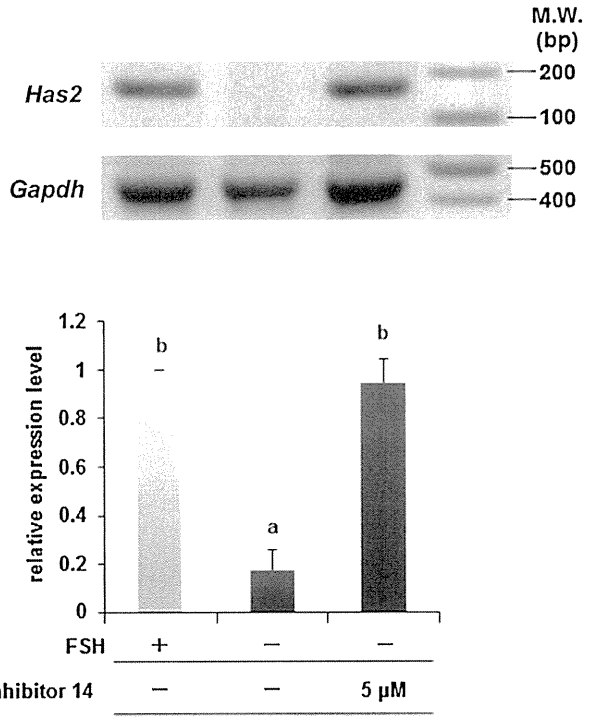

Figure 5. Effect of an FAK Tyr397 phosphorylation inhibitor on the expression of *Has2* mRNA in cumulus cells. The upper panel shows a gel of amplified *Has2* mRNA. The right-most lane contains the molecular markers. The lower bar graph shows relative *Has2* mRNA expression in the presence of FSH or FAK inhibitor. Values shown are means ± standard deviations. Values with different superscripts (a, b) are significantly different ($P < 0.01$). M.W., molecular weight.

differ significantly. Furthermore, inhibition of FAK phosphorylation at Tyr397 during IVM resulted in meiotic arrest, formation of abnormal nuclei and nuclear condensation. Okamura et al. (2001) showed that FAK was expressed in the oocytes of porcine antral follicles, and suggested that the role of FAK may be to prevent apoptosis in oocytes. Consistent with this observation, the FAK/PI3K-mediated cell survival pathway may target PKB (or Akt) activity (Vivanco and Sawyers, 2002), whose signal is transduced into changes in expression of BCL-2-associated X protein (BAX) and BCL-2-like protein 1 (BCL2L1), which are important players in oocyte apoptotic pathways (Jin et al., 2005). In this study, we frequently observed meiotic arrest or nuclear condensation in the oocytes treated with FAK inhibitor 14 at less than 100 μM, a concentration at which non-apoptotic cell death was induced (Golubovskaya et al., 2008); such nuclear condensation is well-associated with cellular apoptosis (Enari et al., 1998; Susin et al., 2000). Taken together, these results implicate FAK and its Tyr397-phosphorylated form in retaining the nuclear status of oocytes.

FAK functions in a variety of cellular events. For example, spindle translocation depends on the cytoplasmic meshwork of F-actin filaments (Longo and Chen, 1985). FAK is known to directly bind to actin-related protein (ARP) 3 and to enhance ARP2/3-dependent actin polymerization (Serrels et al., 2007), whereby the ARP2/3 complex promotes the addition of actin monomers at filament branch points (Svitkina and Borisy, 1999). Thus, FAK may participate in spindle migration by regulating the organization of actin filaments in oocytes. Proline-rich tyrosine kinase 2 (PYK2), which has a domain arrangement similar to FAK, is known to localize to the cell cortex in rat oocytes and to co-localize with actin microfilaments at several developmental stages during oocyte maturation (Meng et al., 2006). Furthermore, PYK2 plays an important role in microfilament assembly in the oocyte, as demonstrated by microinjecting function-blocking anti-PYK2 antibody (Meng et al., 2006). In zebrafish oocytes, activated PYK2, including the Tyr402-phosphorylated form that corresponds to phosphorylated Tyr397 FAK, became more concentrated and closely associated with actin filament bundles structurally supporting the fertilization cone (Sharma and Kinsey, 2013). In mice, FAK is localized in small punctate structures throughout the ooplasm before fertilization; once sperm was incorporated, Tyr861-phosphorylated FAK was concentrated throughout the oocyte cortex, co-localizing with actin layers (McGinnis et al., 2013). In this study, we did not detect significant cortical localization of total or Tyr397-phosphorylated FAK in oocytes from GV to MII stage, and did not examine the association of their localization with the fertilization process. Phosphorylation of FAK at Tyr861, a major site targeted by SRC kinase when bound to Tyr397-phosphorylated FAK (Calalb et al., 1996), is implicated in F-actin organization (Lunn et al., 2007). Therefore, further studies examining the relations among FAK phosphorylation at Tyr397 and Tyr861 and actin filament will reveal important role(s) of FAK in oocyte maturation and fertilization.

We also observed that inhibition of FAK phosphorylation at Tyr397 induced cumulus expansion and expression of *Has2* mRNA, even though FSH was absent from IVM medium. Cumulus expansion can be induced in vitro by FSH (Eppig 1979; Salustri et al., 1992) and by EGF in mouse, pig, cow, and rabbit (Downs 1989; Singh et al., 1993; Boland and Gosden, 1994; Lorenzo et al., 1994; Lorenzo et al., 1996). FSH stimulates elevated adenosine-3′,5′-cyclic monophosphate (cAMP) levels in cumulus cells (Dekel et al., 1979; Eppig, 1979), followed by the increased synthesis of key enzymes involved in the production of hyaluronan (i.e., HAS2) and the binding of hyaluronan to its receptors, such as prostaglandin-endoperoxidase synthase 2 (PTGS2) and tumor necrosis factor α-induced protein 6 (TNFAIP6) (Richards et al., 2002; Vanderhyden, 2002). cAMP is also known to activate protein kinases, including p38 mitogen-activated protein kinase (MAPK), and protein kinase A (PKA), which induce the expression of EGF-like peptides in cumulus cells and thereby indirectly activate ERK1/2 (Shimada et al., 2006; Yamashita et al., 2007). Activated ERK1/2 was recently shown to promote the dephosphorylation of FAK at Tyr397 by inducing the interaction between FAK and protein tyrosine phosphatase (PTP)-PEST (Zheng et al., 2011). ERK1/2, stimulated indirectly by FSH, could therefore induce the dephosphorylation of FAK at Tyr397 and the subsequent detachment of cumulus cells, thus explaining the surprising cumulus

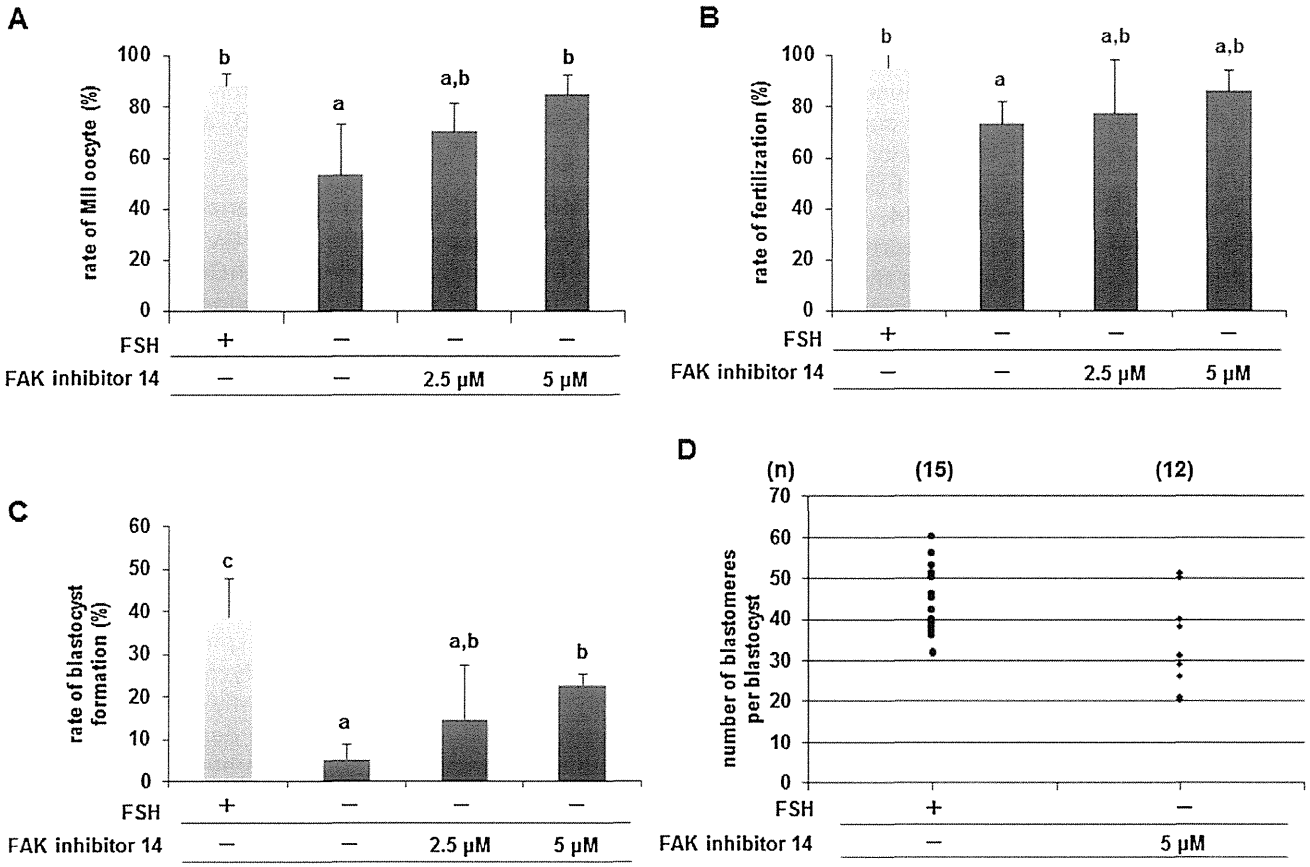

Figure 6. Maturation, fertilization, and development of oocytes treated with a FAK Tyr397 phosphorylation inhibitor. **A:** Rate of maturation to MII oocytes following treatmen with FAK inhibitor 14. **B:** Fertilization rate after IVM. **C:** Rate of blastocyst formation after in vitro fertilization. Bars represent oocytes matured in Waymouth's MB752/1 medium with FSH (white) or FAK inhibitor 14 (black). Values shown are means ± standard deviations. Values with different superscripts (a–c) are significantly different ($P < 0.05$). A total of 77, 54, 58, or 82 oocytes were used in IVM with FSH or 0, 2.5, or 5 μM of FAK inhibitor 14, respectively. **D:** Total number of blastomeres per blastocyst. Numbers in parentheses indicate the number of blastocysts tested per group.

expansion we observed in the presence of FAK inhibitor 14 and the absence of FSH during IVM. On the other hand, ERK1/2 can be regulated by FAK activation when presented with different matrix components (Schlaepfer and Hunter, 1997; Sanders and Basson, 2000; Harnois et al., 2004). In growing fibroblasts, for example, FAK contains phosphotyrosines (Calalb et al., 1995; Schlaepfer and Hunter 1996), but becomes completely dephosphorylated upon cell detachment (Calalb et al., 1995). Considering that contacts among cumulus cells are lost by the accumulation of hyaluronan, it is reasonable to assume that decreased FAK phosphorylation parallels the secretion and accumulation of this matrix protein. Although the molecular relationship between FAK and other factors, including ERK1/2 and HAS2, in cumulus cells is not entirely known, our study provided meaningful insights, including the role of FAK in the induction of cumulus expansion and the regulation of *Has2* mRNA expression by phosphorylation at Tyr397 in mouse cumulus cells.

Treatment of COCs with 5 μM FAK inhibitor 14 during IVM significantly increased the rates of maturation and blastocyst formation compared to those in COCs not treated with FAK inhibitor 14. Bidirectional communication between mammalian oocytes and cumulus cells is essential for the development of both cell types: while fully grown oocytes regulate the proliferation, gene expression, and function of cumulus cells, nutritional support from cumulus cells is essential for the growth and development of these oocytes (Eppig 2001). We found that levels of Tyr397-phosphorylated FAK after in vivo COC maturation are lower in cumulus cells, but not in oocytes, than before maturation. Therefore, we predicted that addition of FAK inhibitor 14, to decrease FAK phosphorylation levels at Tyr397 in cumulus cells during IVM, would have a positive effect on the maturation of cumulus-enclosed oocytes and subsequent embryo development after in vitro fertilization. While there was some benefit, the rate of blastocyst formation remained significantly lower in the presence of 5 μM FAK inhibitor 14 than in the presence of FSH. Thus, cumulus-enclosed oocytes treated with this inhibitor did not achieve the full developmental competence needed to reach the blastocyst stage, which may be why these inhibitor/IVM-derived blastocysts contained fewer blastomeres. The apparent contradiction presented in this study—that FAK

inhibitor decreases oocyte maturation when FSH is present but increases oocyte maturation when FSH is absent —may be explained as follows: FSH induces a low level of Tyr397 FAK phosphorylation that is compatible with oocyte meiotic maturation, and FAK inhibitor 14 can partly mimic this process in the absence of FSH. Combined treatments of FSH and FAK inhibitor 14, however, are too strong for the oocyte, resulting in a decreased maturation rate. Further investigations exploring the relationship between FAK phosphorylation at Tyr397 and other molecules, especially those implicated in FSH-induced signaling pathways, may reveal the function of FAK in oocytes, cumulus cells, and preimplantation embryos. This knowledge should help improve the developmental competence of oocytes by regulating the functions of FAK.

In this study, we demonstrated that FAK expressed in oocytes plays an important role in maintaining nuclear status during meiotic maturation, and that Tyr397-phosphorylated FAK regulates cumulus expansion via *Has2* mRNA expression. Our results also suggest that inhibition of Tyr397 phosphorylation during IVM has a similar effect on the signaling pathways that are induced by FSH during oocyte maturation and preimplantation embryo development.

MATERIALS AND METHODS

Animals and Ethics Statement

All ICR mice were purchased from Japan SLC, Inc. (Shizuoka, Japan), and bred in our laboratory. To minimize suffering, the principles of laboratory animal care were followed. All procedures were conducted in accordance with the guidelines of the Committee for the Care and Use of Laboratory Animals for Research of the Graduate School of Agricultural Science (Tohoku University, Japan). Animal protocols used in this study were approved by the Ethics Committee (Permit Number: 2012-001).

Maturation of Cocs In Vivo and In Vitro

To obtain in vivo-matured COCs, immature, 20- to 23-day-old female mice were injected with 5 IU of PMSG (Teikoku Hormone MFG, Tokyo, Japan), followed by 5 IU of hCG (Teikoku Hormone MFG) 48 hr later. Mice were killed by cervical dislocation, and the oviducts were removed at 12 hr post-hCG injection. COCs were collected in Leibovitz's L-15 medium (Invitrogen, Carlsbad, CA) containing 0.1% (w/v) polyvinyl alcohol (PVA) (Sigma, St. Louis, MO), when oocytes in the COCs were at the MII stage.

IVM was performed as described previously (Sakai et al., 2011). Briefly, ovaries were removed 48 hr after the PMSG injection, and COCs were isolated by puncturing the large antral follicles with a 26-gauge needle and then collecting them in Leibovitz's L-15 medium containing 0.1% PVA and 4 mM hypoxanthine (Sigma) when the oocytes in the COCs were at the GV stage. COCs were cultured in Waymouth's MB752/1 medium (Invitrogen) containing 5% (v/v) fetal calf serum (Gemini Bio, West Sacramento, CA), 4 mM hypoxanthine, 100 IU/l FSH (Sigma), 0.23 mM pyruvic acid (Sigma), 75 mg/l penicillin G (Meiji Seika, Tokyo, Japan), and 50 mg/l streptomycin sulfate (Meiji Seika), for 18 hr in a humidified atmosphere containing 5% (v/v) CO_2 at 37 °C.

Collection of COCs, Oocytes, and Cumulus Cells

Oocyte stages were defined as GV (48 hr after PMSG, i.e., hCG 0 hr) and MII (18 hr after hCG in vivo or 18 hr of IVM). The COC and cumulus-cell stages were defined as before cumulus expansion (hCG 0 hr) and after expansion (12 hr after hCG in vivo or 12–18 hr of IVM). Cumulus cells were separated from their oocytes before and after cumulus expansion by pipetting and by treatment with 0.1% (w/v) hyaluronidase (Sigma) at room temperature. Oocytes that had extruded their first polar body were defined as mature MII-stage oocytes.

Western Blotting

Levels of total and Tyr397-phosphorylated FAK in cumulus cells and oocytes were analyzed as described previously (Sakurai et al., 2012). Briefly, lysates of cumulus cells isolated from 30 COCs or 60 denuded oocytes were loaded into each lane and separated by SDS–PAGE. Separated proteins were transferred to polyvinylidene fluoride membranes (Millipore, Billerica, MA). Membranes were incubated overnight at 4 °C with antibodies against total FAK (1:2000) (Abcam, Cambridge, UK), Tyr397-phosphorylated FAK (1:2000) (Invitrogen) or β-actin (1:5000) (Santa Cruz Biotechnology, Santa Cruz, CA), followed by incubation with appropriate horseradish peroxidase-conjugated secondary antibodies. Probes were detected using the ECL Plus Western blot detection system (GE Healthcare, Little Chalfont, UK). The density of the bands representing total FAK and Tyr397-phosphorylated FAK was normalized to that of β-actin; these relative expression values were presented and used for statistical analysis. Experiments were replicated five or four times for cumulus cells or oocytes, respectively.

Immunocytochemistry

Immunolocalization of total and Tyr397-phosphorylated FAK in COCs and denuded oocytes was performed as described previously (Kogasaka et al., 2013). Briefly, collected COCs or oocytes were fixed and permeabilized with 2% (w/v) paraformaldehyde (Sigma) in phosphate-buffered saline (Nissui Pharmaceutical Co., Tokyo, Japan) containing 0.1% PVA and 0.2% (v/v) Triton X-100 (Wako Pure Chemical Industries, Osaka, Japan) at room temperature for 30 min. They were incubated overnight at 4 °C with rabbit anti-total FAK or rabbit anti-Tyr397-phosphorylated FAK, or for 1 hr at room temperature with mouse anti-α-tubulin (for oocytes; Sigma) antibodies. Then, samples were probed with Alexa Fluor 488-labeled IgG (Molecular probes, Eugene, OR) and counterstained with 10 μg/ml propidium iodide (Sigma). Stained COCs and oocytes were observed using a LSM 700 confocal microscope system

(Carl Zeiss Microimaging, Jena, Germany). Experiments were performed in at least five times.

FAK Inhibitor Treatment During IVM

To inhibit the phosphorylation of FAK at Tyr397, the specific phosphorylation inhibitor FAK inhibitor 14 (Santa Cruz Biotechnology) (Golubovskaya et al., 2008) was added to the IVM medium. We prepared a 50 mM stock solution with sterile distilled water, and diluted it as necessary to a final concentration of 0, 2.5, 5.0, 10, and 25 μM. COCs were cultured for 18 hr to obtain MII oocytes.

Quantification of Cumulus Expansion

Digital images were obtained from COCs and spatial measurements were recorded with Motic Images Plus 2.0S (Shimadzu, Kyoto, Japan). Relative cumulus expansion, defined as the ratio of the greatest distance across the COC expanded matrix (Sutton-McDowall et al., 2004; Yamashita et al., 2011) to the diameter of the oocytes inside them, was calculated for each COC after 18 hr of IVM. Experiments were performed in triplicate.

Reverse-transcriptase Polymerase Chain Reaction

Total RNA extraction and cDNA synthesis were performed as described previously (Sakai et al., 2011), with slight modification. Total RNA was extracted from cumulus cells isolated from 20 COCs after 6 hr of IVM, and cDNA was synthesized using Cells-to-cDNA™ II (Ambion, Austin, TX). PCR was performed using Ex Taq polymerase (TaKaRa Bio, Shiga, Japan) with the following primer pairs: *Has2* sense, 5′-AAGACCC-TATGGTTGGAGGTGTT, and antisense, 5′-CATTCC-CAGAGGACCGCTTAT (167 bp); glyceraldehyde-3-phosphate dehydrogenase (*Gapdh*) (internal standard) sense, 5′-ACCACAGTCCATGCCATCAC, and antisense, 5′-TCCACCACCCTGTTGCTGTA (452 bp). Amplification conditions were as follows: 94 °C for 10 min, followed by 35 cycles of denaturation at 94 °C for 30 sec, annealing at 57 °C (*Has2*) or 58 °C (*Gapdh*) for 30 sec, and extension at 72 °C for 30 sec with a final extension at 72 °C for 5 min. PCR products were electrophoresed on 2% (w/v) agarose gels (Nippon Gene, Tokyo, Japan) and visualized with ethidium bromide (Wako) staining. The density of the band for *Has2* was normalized to the band for *Gapdh*, and the results were statistically analyzed. Experiments were performed in triplicate.

In Vitro Fertilization and In Vitro Culture

In vitro fertilization and embryo culture were performed as described previously (Sakurai et al., 2014). The rates of fertilization (sperm penetration and the formation of two pronuclei) 4 hr after insemination in human tubal fluid (HTF) medium and blastocyst formation 120 hr after embryo culture in potassium simplex optimized medium (KSOM) were analyzed. Experiments were replicated four times.

Blastocyst Cell Counting

Presumptive blastocysts with cavities were fixed for 10 min at room temperature and stained with Hoechst 33342 (5 μg/ml; Sigma) for 10 min at room temperature. Total cell numbers were counted using a LSM700 confocal microscope, and embryos with more than 20 cells were defined as blastocysts.

Statistical Analysis

Significant differences in western blots were calculated using the Student's *t*-test. Statistical differences in maturation, fertilization, and blastocyst formation; relative cumulus expansion; and reverse-transcriptase PCR analysis were determined using one-way ANOVA, followed by Fisher's protected least significant differences (PLSD) test. Statistical significance was evaluated using STATVIEW (Abacus Concepts, Inc., Berkeley, CA).

ACKNOWLEDGMENTS

This work was supported by a grant from the Japan Society for the Promotion of Science to E.S. (No. 24248047). This work was also supported in part by a Grant-in-Aid for Young Scientists (B) from the Ministry of Education, Science, and Culture, Japan to Y.H. (No. 21780250) and by JSPS KAKENHI to Y.H. (No. 26712022).

REFERENCES

Barboni B, Mattioli M, Gioia L, Turriani M, Capacchietti G, Berardinelli P, Bernabo N. 2002. Preovulatory rise of NGF in ovine follicular fluid: Possible involvement in the control of oocyte maturation. Microsc Res Tech 59:516–521.

Biggers JD, Whittingham DG, Donahue RP. 1967. The pattern of energy metabolism in the mouse oocyte and zygote. Proc Natl Acad Sci USA 58:560–567.

Boland NI, Gosden RG. 1994. Effects of epidermal growth factor on the growth and differentiation of cultured mouse ovarian follicles. J Reprod Fertil 101:369–374.

Calalb MB, Polte TR, Hanks SK. 1995. Tyrosine phosphorylation of focal adhesion kinase at sites in the catalytic domain regulates kinase activity: A role for Src family kinases. Mol Cell Biol 15:954–963.

Calalb MB, Zhang X, Polte TR, Hanks SK. 1996. Focal adhesion kinase tyrosine-861 is a major site of phosphorylation by Src. Biochem Biophys Res Commun 228:662–668.

Carpenter G, Cohen S. 1990. Epidermal growth factor. J Biol Chem 265:7709–7712.

Chan PC, Lai JF, Cheng CH, Tang MJ, Chiu CC, Chen HC. 1999. Suppression of ultraviolet irradiation-induced apoptosis by overexpression of focal adhesion kinase in Madin–Darby canine kidney cells. J Biol Chem 274:26901–26906.

Chen HC, Appeddu PA, Isoda H, Guan JL. 1996. Phosphorylation of tyrosine 397 in focal adhesion kinase is required for binding phosphatidylinositol 3-kinase. J Biol Chem 271:26329–26334.

Chen L, Russell PT, Larsen WJ. 1993. Functional significance of cumulus expansion in the mouse: Roles for the preovulatory synthesis of hyaluronic acid within the cumulus mass. Mol Reprod Dev 34:87–93.

Cobb BS, Schaller MD, Leu TH, Parsons JT. 1994. Stable association of pp60src and pp59fyn with the focal adhesion-associated protein tyrosine kinase, pp125FAK. Mol Cell Biol 14:147–155.

Dekel N, Hillensjo T, Kraicer PF. 1979. Maturational effects of gonadotropins on the cumulus-oocyte complex of the rat. Biol Reprod 20:191–197.

Downs SM. 1989. Specificity of epidermal growth factor action on maturation of the murine oocyte and cumulus oophorus in vitro. Biol Reprod 41:371–379.

Enari M, Sakahira H, Yokoyama H, Okawa K, Iwamatsu A, Nagata S. 1998. A caspase-activated DNase that degrades DNA during apoptosis, and its inhibitor ICAD. Nature 391:43–50.

Eppig JJ. 1979. FSH stimulates hyaluronic acid synthesis by oocyte-cumulus cell complexes from mouse preovulatory follicles. Nature 281:483–484.

Eppig JJ. 1991. Intercommunication between mammalian oocytes and companion somatic cells. Bioessays 13:569–574.

Eppig JJ. 2001. Oocyte control of ovarian follicular development and function in mammals. Reproduction 122:829–838.

Fulop C, Salustri A, Hascall VC. 1997. Coding sequence of a hyaluronan synthase homologue expressed during expansion of the mouse cumulus-oocyte complex. Arch Biochem Biophys 337:261–266.

Gardner DK, Pawelczynski M, Trounson AO. 1996. Nutrient uptake and utilization can be used to select viable day 7 bovine blastocysts after cryopreservation. Mol Reprod Dev 44:472–475.

Girault JA, Costa A, Derkinderen P, Studler JM, Toutant M. 1999. FAK and PYK2/CAKbeta in the nervous system: A link between neuronal activity, plasticity and survival. Trends Neurosci 22:257–263.

Goel HL, Dey CS. 2002. Focal adhesion kinase tyrosine phosphorylation is associated with myogenesis and modulated by insulin. Cell Prolif 35:131–142.

Golubovskaya VM, Nyberg C, Zheng M, Kweh F, Magis A, Ostrov D, Cance WG. 2008. A small molecule inhibitor, 1,2,4,5-benzenetetraamine tetrahydrochloride, targeting the y397 site of focal adhesion kinase decreases tumor growth. J Med Chem 51:7405–7416.

Hanks SK, Polte TR. 1997. Signaling through focal adhesion kinase. Bioessays 19:137–145.

Harnois C, Demers MJ, Bouchard V, Vallee K, Gagne D, Fujita N, Tsuruo T, Vezina A, Beaulieu JF, Cote A, Vachon PH. 2004. Human intestinal epithelial crypt cell survival and death: Complex modulations of Bcl-2 homologs by Fak, PI3-K/Akt-1, MEK/Erk, and p38 signaling pathways. J Cell Physiol 198:209–222.

Hess KA, Chen L, Larsen WJ. 1999. Inter-alpha-inhibitor binding to hyaluronan in the cumulus extracellular matrix is required for optimal ovulation and development of mouse oocytes. Biol Reprod 61:436–443.

Hsieh M, Lee D, Panigone S, Horner K, Chen R, Theologis A, Lee DC, Threadgill DW, Conti M. 2007. Luteinizing hormone-dependent activation of the epidermal growth factor network is essential for ovulation. Mol Cell Biol 27:1914–1924.

Igishi T, Fukuhara S, Patel V, Katz BZ, Yamada KM, Gutkind JS. 1999. Divergent signaling pathways link focal adhesion kinase to mitogen-activated protein kinase cascades. Evidence for a role of paxillin in c-Jun NH(2)-terminal kinase activation. J Biol Chem 274:30738–30746.

Jin X, Han CS, Yu FQ, Wei P, Hu ZY, Liu YX. 2005. Anti-apoptotic action of stem cell factor on oocytes in primordial follicles and its signal transduction. Mol. Reprod Dev 70:82–90.

Judson PL, He X, Cance WG, Van Le L. 1999. Overexpression of focal adhesion kinase, a protein tyrosine kinase, in ovarian carcinoma. Cancer 86:1551–1556.

Khamsi F, Armstrong DT. 1997. Interactions between follicle-stimulating hormone and growth factors in regulation of deoxyribonucleic acid synthesis in bovine granulosa cells. Biol Reprod 57:684–688.

Kidder GM, Mhawi AA. 2002. Gap junctions and ovarian folliculogenesis. Reproduction 123:613–620.

Kogasaka Y, Hoshino Y, Hiradate Y, Tanemura K, Sato E. 2013. Distribution and association of mTOR with its cofactors, raptor and rictor, in cumulus cells and oocytes during meiotic maturation in mice. Mol Reprod Dev 80:334–348.

Longo FJ, Chen DY. 1985. Development of cortical polarity in mouse eggs: Involvement of the meiotic apparatus. Dev Biol 107:382–394.

Lorenzo PL, Illera MJ, Illera JC, Illera M. 1994. Enhancement of cumulus expansion and nuclear maturation during bovine oocyte maturation in vitro by the addition of epidermal growth factor and insulin-like growth factor I. J Reprod Fertil 101:697–701.

Lorenzo PL, Rebollar PG, Illera MJ, Illera JC, Illera M, Alvarino JM. 1996. Stimulatory effect of insulin-like growth factor I and epidermal growth factor on the maturation of rabbit oocytes in vitro. J Reprod Fertil 107:109–117.

Lunn JA, Jacamo R, Rozengurt E. 2007. Preferential phosphorylation of focal adhesion kinase tyrosine 861 is critical for mediating an anti-apoptotic response to hyperosmotic stress. J Biol Chem 282:10370–10379.

Luo J, McGinnis LK, Kinsey WH. 2009. Fyn kinase activity is required for normal organization and functional polarity of the mouse oocyte cortex. Mol Reprod Dev 76:819–831.

McGinnis LK, Albertini DF, Kinsey WH. 2007. Localized activation of Src-family protein kinases in the mouse egg. Dev Biol 306:241–254.

McGinnis LK, Luo J, Kinsey WH. 2013. Protein tyrosine kinase signaling in the mouse oocyte cortex during sperm-egg interactions and anaphase resumption. Mol Reprod Dev 80: 260–272.

Meng XQ, Zheng KG, Yang Y, Jiang MX, Zhang YL, Sun QY, Li YL. 2006. Proline-rich tyrosine kinase2 is involved in F-actin organization during in vitro maturation of rat oocyte. Reproduction 132:859–867.

Mitra SK, Hanson DA, Schlaepfer DD. 2005. Focal adhesion kinase: In command and control of cell motility. Nat Rev Mol Cell Biol 6:56–68.

Mizutani T, Shiraishi K, Welsh T, Ascoli M. 2006. Activation of the lutropin/choriogonadotropin receptor in MA-10 cells leads to the tyrosine phosphorylation of the focal adhesion kinase by a pathway that involves Src family kinases. Mol Endocrinol 20:619–630.

Nagano M, Hoshino D, Koshikawa N, Akizawa T, Seiki M. 2012. Turnover of focal adhesions and cancer cell migration. Int J Cell Biol 2012:310616.

Noma N, Kawashima I, Fan HY, Fujita Y, Kawai T, Tomoda Y, Mihara T, Richards JS, Shimada M. 2011. LH-induced neuregulin 1 (NRG1) type III transcripts control granulosa cell differentiation and oocyte maturation. Mol Endocrinol 25:104–116.

Okamura Y, Myoumoto A, Manabe N, Tanaka N, Okamura H, Fukumoto M. 2001. Protein tyrosine kinase expression in the porcine ovary. Mol Hum Reprod 7:723–729.

Owen JD, Ruest PJ, Fry DW, Hanks SK. 1999. Induced focal adhesion kinase (FAK) expression in FAK-null cells enhances cell spreading and migration requiring both auto- and activation loop phosphorylation sites and inhibits adhesion-dependent tyrosine phosphorylation of Pyk2. Mol Cell Biol 19:4806–4818.

Owen KA, Pixley FJ, Thomas KS, Vicente-Manzanares M, Ray BJ, Horwitz AF, Parsons JT, Beggs HE, Stanley ER, Bouton AH. 2007. Regulation of lamellipodial persistence, adhesion turnover, and motility in macrophages by focal adhesion kinase. J Cell Biol 179:1275–1287.

Park JY, Su YQ, Ariga M, Law E, Jin SL, Conti M. 2004. EGF-like growth factors as mediators of LH action in the ovulatory follicle. Science 303:682–684.

Pelech S, Jelinkova L, Susor A, Zhang H, Shi X, Pavlok A, Kubelka M, Kovarova H. 2008. Antibody microarray analyses of signal transduction protein expression and phosphorylation during porcine oocyte maturation. J Proteome Res 7:2860–2871.

Preis KA, Seidel G, Jr., Gardner DK. 2005. Metabolic markers of developmental competence for in vitro-matured mouse oocytes. Reproduction 130:475–483.

Richards JS, Russell DL, Ochsner S, Hsieh M, Doyle KH, Falender AE, Lo YK, Sharma SC. 2002. Novel signaling pathways that control ovarian follicular development, ovulation, and luteinization. Recent Prog Horm Res 57:195–220.

Russell DL, Robker RL. 2007. Molecular mechanisms of ovulation: Co-ordination through the cumulus complex. Hum Reprod Update 13:289–312.

Sakai C, Hoshino Y, Sato Y, Sato E. 2011. Evaluation of maturation competence of metaphase II oocytes in mice based on the distance between pericentriolar materials of meiotic spindle: distance of PCM during oocyte maturation. J Assist Reprod Genet 28:157–166.

Sakurai M, Ohtake J, Ishikawa T, Tanemura K, Hoshino Y, Arima T, Sato E. 2012. Distribution and Y397 phosphorylation of focal adhesion kinase on follicular development in the mouse ovary. Cell Tissue Res 347:457–465.

Sakurai M, Sato Y, Mukai K, Suematsu M, Fukui E, Yoshizawa M, Tanemura K, Hoshino Y, Matsumoto H, Sato E. 2014. Distribution of tubulointerstitial nephritis antigen-like 1 and structural matrix proteins in mouse embryos during preimplantation development in vivo and in vitro. Zygote 22:259–265.

Salustri A, Yanagishita M, Underhill CB, Laurent TC, Hascall VC. 1992. Localization and synthesis of hyaluronic acid in the cumulus cells and mural granulosa cells of the preovulatory follicle. Devel Biol 151:541–551.

Sanders MA, Basson MD. 2000. Collagen IV-dependent ERK activation in human Caco-2 intestinal epithelial cells requires focal adhesion kinase. Journal Biol Chem 275:38040–38047.

Schaller MD, Borgman CA, Cobb BS, Vines RR, Reynolds AB, Parsons JT. 1992. pp125FAK a structurally distinctive protein-tyrosine kinase associated with focal adhesions. Proc Natl Acad Sci USA 89:5192–5196.

Schaller MD, Hildebrand JD, Shannon JD, Fox JW, Vines RR, Parsons JT. 1994. Autophosphorylation of the focal adhesion kinase, pp125FAK, directs SH2-dependent binding of pp60src. Mol Cell Biol 14:1680–1688.

Schlaepfer DD, Hanks SK, Hunter T, van der Geer P. 1994. Integrin-mediated signal transduction linked to Ras pathway by GRB2 binding to focal adhesion kinase. Nature 372:786–791.

Schlaepfer DD, Hunter T. 1996. Evidence for in vivo phosphorylation of the Grb2 SH2-domain binding site on focal adhesion kinase by Src-family protein-tyrosine kinases. Mol Cell Biol 16:5623–5633.

Schlaepfer DD, Hunter T. 1997. Focal adhesion kinase overexpression enhances ras-dependent integrin signaling to ERK2/mitogen-activated protein kinase through interactions with and activation of c-Src. J Biol Chem 272:13189–13195.

Schwartz MA, Schaller MD, Ginsberg MH. 1995. Integrins: Emerging paradigms of signal transduction. Annu Rev Cell Dev Biol 11:549–599.

Serrels B, Serrels A, Brunton VG, Holt M, McLean GW, Gray CH, Jones GE, Frame MC. 2007. Focal adhesion kinase controls

actin assembly via a FERM-mediated interaction with the Arp2/3 complex. Nat Cell Biol 9:1046–1056.

Sharma D, Kinsey WH. 2013. PYK2: A calcium-sensitive protein tyrosine kinase activated in response to fertilization of the zebrafish oocyte. Dev Biol 373:130–140.

Shimada M, Hernandez-Gonzalez I, Gonzalez-Robayna I, Richards JS. 2006. Paracrine and autocrine regulation of epidermal growth factor-like factors in cumulus oocyte complexes and granulosa cells: Key roles for prostaglandin synthase 2 and progesterone receptor. Mol Endocrinol 20:1352–1365.

Singh B, Barbe GJ, Armstrong DT. 1993. Factors influencing resumption of meiotic maturation and cumulus expansion of porcine oocyte–cumulus cell complexes in vitro. Mol Reprod Dev 36:113–119.

Sirotkin AV, Dukesova J, Pivko J, Makarevich AV, Kubek A. 2002. Effect of growth factors on proliferation, apoptosis and protein kinase A expression in cultured porcine cumulus oophorus cells. Reprod Nutr Dev 42:35–43.

Sonoda Y, Matsumoto Y, Funakoshi M, Yamamoto D, Hanks SK, Kasahara T. 2000. Anti-apoptotic role of focal adhesion kinase (FAK). Induction of inhibitor-of-apoptosis proteins and apoptosis suppression by the overexpression of FAK in a human leukemic cell line, HL-60. J Biol Chem 275:16309–16315.

Sood AK, Coffin JE, Schneider GB, Fletcher MS, DeYoung BR, Gruman LM, Gershenson DM, Schaller MD, Hendrix MJ. 2004. Biological significance of focal adhesion kinase in ovarian cancer: Role in migration and invasion. Am J Pathol 165:1087–1095.

Susin SA, Daugas E, Ravagnan L, Samejima K, Zamzami N, Loeffler M, Costantini P, Ferri KF, Irinopoulou T, Prevost MC, Brothers G, Mak TW, Penninger J, Earnshaw WC, Kroemer G. 2000. Two distinct pathways leading to nuclear apoptosis. J Exp Med 192:571–580.

Sutton-McDowall ML, Gilchrist RB, Thompson JG. 2004. Cumulus expansion and glucose utilisation by bovine cumulus-oocyte complexes during in vitro maturation: The influence of glucosamine and follicle-stimulating hormone. Reproduction 128:313–319.

Svitkina TM, Borisy GG. 1999. Arp2/3 complex and actin depolymerizing factor/cofilin in dendritic organization and treadmilling of actin filament array in lamellipodia. J Cell Biol 145: 1009–1026.

Thomas SM, Brugge JS. 1997. Cellular functions regulated by Src family kinases. Annu Rev Cell Dev Biol 13:513–609.

Vanderhyden B. 2002. Molecular basis of ovarian development and function. Front Biosci 7:d2006–2022.

Vivanco I, Sawyers CL. 2002. The phosphatidylinositol 3-Kinase AKT pathway in human cancer. Nat Rev Cancer 2:489–501.

Wang HB, Dembo M, Hanks SK, Wang Y. 2001. Focal adhesion kinase is involved in mechanosensing during fibroblast migration. Proc Natl Acad Sci U S A 98:11295–11300.

Yamashita Y, Kawashima I, Yanai Y, Nishibori M, Richards JS, Shimada M. 2007. Hormone-induced expression of tumor necrosis factor alpha-converting enzyme/A disintegrin and metalloprotease-17 impacts porcine cumulus cell oocyte complex expansion and meiotic maturation via ligand activation of the epidermal growth factor receptor. Endocrinology 148:6164–6175.

Yamashita Y, Okamoto M, Kawashima I, Okazaki T, Nishimura R, Gunji Y, Hishinuma M, Shimada M. 2011. Positive feedback loop between prostaglandin E2 and EGF-like factors is essential for sustainable activation of MAPK3/1 in cumulus cells during in vitro maturation of porcine cumulus oocyte complexes. Biol Reprod 85:1073–1082.

Zachary I, Rozengurt E. 1992. Focal adhesion kinase (p125FAK): A point of convergence in the action of neuropeptides, integrins, and oncogenes. Cell 71:891–894.

Zheng KG, Meng XQ, Yang Y, Yu YS, Liu DC, Li YL. 2007. Requirements of Src family kinase during meiotic maturation in mouse oocyte. Mol Reprod Dev 74:125–130.

Zheng Y, Yang W, Xia Y, Hawke D, Liu DX, Lu Z. 2011. Ras-induced and extracellular signal-regulated kinase 1 and 2 phosphorylation-dependent isomerization of protein tyrosine phosphatase (PTP)-PEST by PIN1 promotes FAK dephosphorylation by PTP-PEST. Mol Cell Biol 31:4258–4269.

SUPPORTING INFORMATION

Additional supporting information may be found in the online version of this article at the publisher's web-site.

MRD

Journal of Reproduction and Development, Vol. 60, No 5, 2014

—Original Article—

Histone H4 Modification During Mouse Spermatogenesis

Yoshiki SHIRAKATA[1)], Yuuki HIRADATE[1)], Hiroki INOUE[1)], Eimei SATO[2)] and Kentaro TANEMURA[1)]

[1)]*Laboratory of Animal Reproduction and Development, Graduate School of Agricultural Science, Tohoku University, Sendai 981-8555, Japan*

[2)]*National Livestock Breeding Center, Fukushima 961-8511, Japan*

Abstract. The core histone is composed of four proteins (H2A, H2B, H3 and H4). Investigation of the modification patterns of histones is critical to understanding their roles in biological processes. Although histone modification is observed in multiple cells and tissues, little is known about its function in spermatogenesis. We focused on the modification patterns of histone H4 during murine spermatogenesis. We demonstrated that the individual N-terminal sites of H4 show different modification patterns during the differentiation of male germ cells. The methylation pattern varied depending on the residues that were mono-, di-, or tri-methylated. All the H4 modifications were high during the meiotic prophase, suggesting that histone H4 modification plays an important role during this stage of spermatogenesis. Elongating spermatids showed increased acetylation of histone H4, which may be associated with a histone-to-protamine substitution. Our results provide further insight into the specific relationship between histone H4 modification and gene expression during spermatogenesis, which could help to elucidate the epigenetic disorders underlying male infertility.

Key words: Acetylation, Histone H4, Immunohistochemistry, Mouse, Spermatogenesis

(**J. Reprod. Dev.** 60: 383–387, 2014)

Epigenetics is the study of mitotically or meiotically heritable changes in gene expression or cellular phenotype that are caused by mechanisms other than changes in the underlying DNA sequence [1]. As an epigenetic mechanism, histone modification is as important as DNA methylation and plays essential roles in gene inactivation and activation. The core histone is composed of four proteins (H2A, H2B, H3 and H4), and their N-terminal ends can be chemically modified by methylation, acetylation, and phosphorylation [2]. These modifications change the chromatin structure, thereby influencing gene expression [3–5]. Histone methylation is associated with transcriptional activation and inactivation, depending on the histone N-terminal residues involved [6]. Histone acetylation is associated with the activation of gene expression [7, 8], while histone phosphorylation is related to transcriptional activation. Histone modification is a reversible process catalyzed by enzymes such as methyltransferases, demethylases, acetyltransferases and deacetyltransferases [9, 10].

During the process of female germ cell differentiation, histone modification patterns undergo dramatic changes [11–16] that play an important role in oocyte maturation and oogenesis. In comparison, the effect of histone modification on the differentiation of male germ cells remains understudied.

Spermatogenesis is a very unique cell differentiation process, in that it consists of gene recombination, meiosis and the exchange from histones to protamines. Histone modification patterns during spermatogenesis have been reported to perform specific roles [17, 18]. Although the role of histone H3 modifications during spermatogenesis has been examined [19], the functions of the other histone proteins are unknown. Therefore, our research focused on the histone H4 protein. Histone H4 can be acetylated at lysine 5, 8, 12 and 16 and methylated at arginine 3 and lysine 20 on its N-terminal tail. Histone H4 modifications are involved in the regulation of chromatin structure, protein-protein interactions and transcriptional activity through the nuclear hormone receptor [20–23]. In this study, we used immunohistochemical techniques to analyze the modification of histone H4 during spermatogenesis.

Materials and Methods

Animals

We purchased 12-week-old male C57/BL6 mice from SLC (Shizuoka, Japan). The mice were anesthetized with 2,2,2-tribromoethanol. Their testes were surgically removed, fixed with the methacarn fixative (methanol:chloroform:acetic acid = 6:3:1), treated with 100% ethanol and xylene, and then embedded in paraffin. The care and use of all the mice conformed to the Regulations for Animal Experiments and Related Activities at Tohoku University.

Antibodies

Mouse monoclonal antibodies against histone H4 mono-methylation (H4me, sc-134221: Santa Cruz Biotechnology, Santa Cruz, CA, USA) and histone H4 tri-methylation (H4me3, sc-134216; Santa Cruz Biotechnology) and rabbit polyclonal antibodies against histone H4 lysine 5 acetylation (H4K5ac, sc-34264: Santa Cruz Biotechnology), histone H4 lysine 8 acetylation (H4K8ac, sc-8661-R: Santa Cruz

Received: February 6, 2014
Accepted: June 27, 2014
Published online in J-STAGE: August 2, 2014

Correspondence: K Tanemura (e-mail: kentaro@m.tohoku.ac.jp)